A numerical flume for waves on variable sheared currents using smoothed particle hydrodynamics (SPH) with open boundaries

DOI:
10.1016/j.apor.2023.103527

Document Version
Final published version

Applied Ocean Research 135 (2023) 103527

Contents lists available at ScienceDirect

Applied Ocean Research

journal homepage: www.elsevier.com/locate/apor

A numerical flume for waves on variable sheared currents using smoothed particle hydrodynamics (SPH) with open boundaries

Yong Yang *, Samuel Draycott, Peter K. Stansby, Benedict D. Rogers

Department of Mechanical, Aerospace and Civil Engineering, University of Manchester, Manchester M13 9PL, UK

ARTICLE INFO

Keywords:
Wave-current flume
Wave-current interaction
Sheared currents
Open boundary conditions
Smoothed particle hydrodynamics
DualSPHysics

ABSTRACT

Combinations of waves and currents exist in a wide range of marine environments. The resulting, often complex, combined wave-current conditions largely determine the loading, response and survivability of vessels, offshore platforms and systems. Smoothed Particle Hydrodynamics (SPH) has becoming increasingly popular for free-surface flow problems which do not require special treatment to detect the free surface. The present work implements open boundaries for wave-current conditions within the SPH-based DualSPHysics solver. Open boundaries are applied for the generation of wave-alone, current-alone and combined wave-current conditions. A modified damping zone acting on the vertical velocity component is used for wave absorption and combined with open boundaries to allow particles to leave or enter the fluid domain when a current exists. Results of wave-alone (regular, irregular and focused) and current-alone (uniform, linearly sheared and arbitrary sheared) test cases demonstrate a general numerical flume is achieved. Tests of focused waves interacting with arbitrary sheared currents are validated with analytical linear solutions for surface elevation and velocities, demonstrating excellent agreement. The numerical flume may be extended to steep waves well suited to SPH and thus enable modelling complex and extreme wave-current conditions interacting with offshore platforms and systems.

1. Introduction

Offshore renewable energy has gradually become an important source to satisfy the rapidly increasing demand for energy. A wide range of natural locations for deployment of offshore renewable energy (ORE) systems experience combinations of waves and currents, especially in nearshore and coastal regions. Wave-current conditions largely determine the loading and response of offshore structures (Bruserud et al., 2018). These conditions bring challenges for the design of offshore structures including ORE systems, partly due to difficulties in the understanding and modelling of such conditions, and partly due to the nature of the combined conditions themselves. To ensure a proper design of ORE systems to withstand such complex wave-current conditions, it is of great significance to understand the range and likelihood of different conditions and to be able to model them effectively.

Wave characteristics are modified in the presence of current (e.g., Jonsson et al., 1970; Jonsson, 1990; Smith, 1997). Currents, including the mean vertical profile, are also changed in the presence of waves (e.g., Wolf and Prandle, 1999; Olabarrieta et al., 2010). Wavelengths are lengthened in the presence of a following current and shortened in the presence of an opposing current. Meanwhile, the change in wave amplitude can be inferred by the conservation of wave action (Jonsson, 1990; Smith, 1997). Theoretical studies and developments are important for the modelling of wave-current interactions and can be used to provide appropriate boundary conditions to numerical models. For waves in the presence of a uniform current, analytical solutions for the wave-current field have been found for weakly nonlinear waves. Baddour and Song (1990) obtained the resulting wave-current field described by wave height, wavelength, current speed, and water depth by solving a set of nonlinear equations for waves interacting with the uniform current in finite water depth on a horizontal bed. Jonsson (1990) described a modified dispersion relation to consider the relationship between wavenumber and angular frequency for a linear wave interacting with a uniform current since the wavelengths are modified and are no longer related to the angular frequency observed in the fixed reference frame through the standard dispersion relation. This modified dispersion relation is used in the present study for waves interacting with a uniform current. For waves interacting with a linearly sheared current, wave-current interactions have been also studied theoretically. Choi (2009) derived a series of equations for fully nonlinear waves in the

* Corresponding author.
E-mail address: yong.yang-3@postgrad.manchester.ac.uk (Y. Yang).

https://doi.org/10.1016/j.apor.2023.103527
Received 6 October 2022; Received in revised form 13 January 2023; Accepted 1 March 2023
Available online 29 March 2023

presence of a linearly sheared current with constant vorticity in infinitely deep water to study the effects on waves. Nwogu (2009) presented a novel method to obtain the dispersion relation in sheared currents from the Fourier transform of the evolution equations and the closure relationship. This modified dispersion relation is used in the present study for waves interacting with a linearly sheared current. When the gradient of the vertical profile, and hence the vorticity, varies with the water depth, the interactions between waves and currents are more complicated. Ellingsen and Li (2017) described a theory of approximate dispersion relations considering linear surface waves interacting with an arbitrary sheared current. The magnitude and direction of the sheared current can vary arbitrarily as a function of water depth. A direct integration method (DIM) developed by Li and Ellingsen (2019) allows accurate evaluation of surface waves in the presence of a current of arbitrary profile. In particular, the efficient evaluation of the dispersion relation for linear surface waves interacting with an arbitrary sheared current on the horizontally constant water depth was included in the DIM. This method is used in the present study for waves interacting with an arbitrary sheared current defined by a power law profile.

Experiments provide an effective approach for both fundamental studies into wave-current conditions and also applied problems associated with the behavior of offshore systems in such conditions. The effects of a depth-varying current velocity with non-uniform vorticity distribution on the waves was studied in Swan et al. (2001), where it was concluded that the vorticity distribution can significantly change the water-surface profile and plays an important role in determining the overall wave height change in the current. An experimental study on the incipient breaking of unsteady waves on sheared currents was described in Yao and Wu (2005). The steepness at the breaking threshold was found to reduce proportionally to the strength of a positively sheared current and increase proportionally to a negatively sheared current. Waves interacting with an opposing current were studied in Toffoli et al. (2013) and Ma et al. (2013) concluding that stable wave trains may become modulationally unstable and trigger rogue wave events. The dispersion and modulational instability of waves on opposing linearly sheared current with constant vorticity was experimentally studied in Steer et al. (2020). The experimental results were compared against the numerical solutions from the constant vorticity nonlinear Schrödinger equation (the vor-NLSE) in Thomas et al. (2012) and showed that the vor-NLSE give better results than the uniform-current NLSE. Experimental investigations are widely carried out in wave-current conditions, in part due to difficulties in modelling such conditions. However, limits exist on how well the conditions observed in the real world can be replicated experimentally since the precise generation of complex and extreme wave conditions in arbitrary currents is not possible in most experimental facilities.

Greater control over wave-current conditions can in principle be achieved in numerical simulations with the appropriate definition of boundary conditions. Numerical simulations may be undertaken to investigate complex and extreme wave-current conditions. Those conditions can generate highly violent and nonlinear flows requiring an appropriate modelling technique. Smoothed Particle Hydrodynamics (SPH) (Gingold and Monaghan, 1977; Lucy, 1977) has received increasing attention and is used to study free-surface flows (Monaghan, 1994; Monaghan and Kos, 1999; Monaghan et al., 1999). As a Lagrangian and meshless technique for Computational Fluid Dynamics (CFD), SPH is ideally suited to fluid problems with large deformation and high nonlinearity (e.g. Dalrymple and Rogers, 2006; Gómez-Gesteira et al., 2010; Lind et al., 2012). The present work uses the DualSPHysics solver which is an open-source SPH code accelerated on a graphics processing unit (Domínguez et al., 2022). Long-crested waves have been simulated within DualSPHysics by Altomare et al. (2017). A piston-type wavemaker was used for wave generation, while both passive and active wave absorption were implemented to avoid wave reflection. The numerical results were validated against both theory and experiments demonstrating good performance. Wave run-up over breakwaters was studied using DualSPHysics in Zhang et al. (2018). The numerical results showed an overall good accuracy for surface elevation, orbital velocities and time series of the run-up after validation with the experiments. An alternative approach for wave generation and wave absorption within DualSPHysics is using open boundary conditions. The implementation of open boundaries in DualSPHysics was presented in Tafuni et al. (2018) and have been applied for the numerical modelling of non-linear waves in Verbrugghe et al. (2019). The results showed that the wave generation and absorption by using open boundary conditions is an efficient and accurate approach in DualSPHysics.

Numerical studies based on SPH for wave-current interactions are rare to date compared with mature mesh-based methods. Based on mesh-based CFD and the Volume-of-Fluid (VOF) method, Markus et al. (2013) investigated the interaction between nonlinear waves and a non-uniform current. The wave was projected onto the current profile gradually at the inlet and then the interaction between the wave and the current was captured. Zhang et al. (2014) developed a Reynolds-Averaged Navier-Stokes (RANS) solver combined with a VOF method for the simulation of wave-current interactions. The wave was generated by an internal wavemaker method in the middle of the domain after a steady current was achieved by imposing an inlet velocity on one end and a pressure outlet on the other end. Numerical studies based on a Navier-Stokes solver combined with the VOF method for modelling waves interacting with the depth varying currents were investigated by Chen and Zou (2019). The water particle velocity at the inlet was specified by a superposition of the current and wave velocities without considering the current modification to the wave kinematics. Some example studies for the wave-current interaction based on mesh-based CFD are introduced above. Compared with using mesh-based CFD, wave-current interaction studies based on SPH are rare and the generation of waves in sheared currents has received no attention to date. The wave-current interaction was simulated using the SPH method by He et al. (2018). Regular waves were simulated using a wavemaker and were absorbed using a sponge layer. The uniform current was generated by simultaneously imposing the directional velocity and hydrostatic pressure in the inflow region and the outflow region below the numerical wave-current flume. Wave-current conditions were simulated by a wavemaker and a circulating current system in Shi et al. (2018) and Liu et al. (2021) to study the hydrodynamic response of a flexible structure using SPH. A numerical wave-current flume based on the SPH method can also be found in Ni et al. (2020). The wave-current interactions were obtained by means of a non-reflective open boundary condition with no wavemakers and sponge layers. Features of regular waves interacting with steady currents and solitary wave-current interaction over a bump were studied. It can be seen that a superposition of the current profile and the current-unmodified wave-induced velocities is often specified at the inlet with the interaction between the wave and the current being captured within a distance from the domain inlet for numerical simulations of wave-current interactions. It is also a general approach for considering the waves interacting with the arbitrary sheared currents. This approach however makes it challenging to specify the combined wave-current field accurately.

In this paper, a numerical wave-current flume is developed using open boundaries within DualSPHysics. Analytical solutions of modified dispersion relations for linear waves interacting with uniform and linearly sheared current are used. For arbitrary sheared currents, solutions of the modified wavenumbers and the modified wave-induced kinematics are obtained using the direct integration method (DIM) of Li and Ellingsen (2019). Based on these solutions, a superposition of the current profile and current-altered wave-induced velocities is imposed at the inlet for wave-current generation using open boundaries. With open boundaries, a damping zone for vertical velocity only is used for wave absorption allowing access for particles to leave or enter the computational domain due to a current. This avoids the requirement for a domain with wave-current interaction to become established with the associated

setup time, and importantly allows for exact specification of the combined conditions. The implementation for generating complex wave-current conditions in this numerical wave-current flume is initially validated with theoretical results for wave-alone (regular, irregular and focused) conditions and current-alone (uniform, linearly sheared and arbitrary sheared) conditions. A convergence study is presented for a focused wave and an opposing linearly sheared current. The interactions between focused waves and arbitrary sheared currents are presented and validated against theoretical solutions for surface elevations and velocities, demonstrating the model's capability for modelling complex wave-current interactions which may impact offshore systems.

This paper is organized as follows: in Section 2, the SPH model is outlined. In Section 3, a description of the methodology for the implementation of the numerical wave-current flume is given. In Section 4, the results of several wave-alone and current-alone test cases are presented. In Section 5, the results of the focused wave interacting with the arbitrary sheared current are given. In Section 6, the conclusions and future work are provided.

2. Smoothed particle hydrodynamics model

SPH is a Lagrangian and meshless method which is increasingly used for solving astrophysics, fluid dynamics and solid mechanics problems (Violeau and Rogers, 2016; Gotoh and Khayyer, 2016; Shadloo et al., 2016; Ye et al., 2019). The solver used for modelling complex wave-current conditions in the present study is the SPH-based DualSPHysics code (Domínguez et al., 2022). In SPH, a function $f(\mathbf{r})$ can be estimated by the integral approximation as follows:

$$f(\mathbf{r}) = \int_{\Omega} f(\mathbf{r}^{'}) W(\mathbf{r}-\mathbf{r}^{'}, h)\mathrm{d}\mathbf{r}^{'} \tag{1}$$

where the integral is over the domain Ω and $W(\mathbf{r}-\mathbf{r}^{'}, h)$ is the kernel function with h defined as the smoothing length. As a meshless method, the fluid is discretised into a set of particles and physical quantities of each particle are computed as the interpolation of the values of the neighbouring particles. In the discrete form, the integral approximation can be transformed approximately as:

$$f(\mathbf{r}_a) \approx \sum_b f(\mathbf{r}_b)\frac{m_b}{\rho_b} W(\mathbf{r}_a-\mathbf{r}_b, h) \tag{2}$$

where m_b/ρ_b is the volume of particle b with m_b and ρ_b being the particle mass and particle density respectively, and $W(\mathbf{r}_a-\mathbf{r}_b, h)$ is the kernel function between particle a and particle b. In the present study, the kernel used is the quintic Wendland kernel (Wendland, 1995) given by:

$$W(r,h) = \alpha_D\left(1-\frac{q}{2}\right)^4(2q+1)\ 0 \le q \le 2 \tag{3}$$

where α_D equals $7/(4\pi h^2)$ and $21/(16\pi h^3)$ in 2-D and 3-D respectively, $q = r/h$ is the non-dimensional distance between particles where r is the distance between particle a and particle b. The smoothing length is set equal to $h = 1.5 \times \sqrt{2} \times d_p$ in the present study with d_p the particle size (the initial interparticle distance is referred to as particle size d_p).

2.1. SPH governing equations

The momentum equation in Lagrangian form can be written as:

$$\frac{\mathrm{d}\mathbf{v}}{\mathrm{d}t} = -\frac{1}{\rho}\nabla P + \mathbf{g} + \Gamma \tag{4}$$

where $\mathbf{g}$ is the gravitational acceleration and Γ refers to dissipative terms. The use of artificial viscosity (Monaghan, 1992) is a common stabilizing method used in SPH and is applied in the present study. In SPH notation, Eq. (4) can be written as:

$$\frac{\mathrm{d}\mathbf{v}_a}{\mathrm{d}t} = -\sum_b m_b\left(\frac{P_b+P_a}{\rho_b\rho_a} + \Pi_{ab}\right)\nabla_a W_{ab} + \mathbf{g} \tag{5}$$

where ρ is density, $\mathbf{v}$ is velocity, t is time, m is mass, P is pressure, $\mathbf{g}$ is gravitational acceleration and W is the kernel function. The viscosity term Π_{ab} is given by:

$$\Pi_{ab} = \begin{cases} \dfrac{-\alpha \bar{c_{ab}}\mu_{ab}}{\bar{\rho_{ab}}} & \mathbf{v}_{ab}\cdot\mathbf{r}_{ab} < 0 \\ 0 & \mathbf{v}_{ab}\cdot\mathbf{r}_{ab} \ge 0 \end{cases} \tag{6}$$

where $\bar{c_{ab}} = (c_a + c_b)/2$ is the mean speed of sound, $\bar{\rho_{ab}} = (\rho_a + \rho_b)/2$, $\mu_{ab} = h\mathbf{v}_{ab}\cdot\mathbf{r}_{ab}/(r_{ab}^2 + 0.01h^2)$, α is the coefficient depending on the problem to provide proper dissipation. In the present study, the value 0.01 is selected (Altomare et al., 2015). The continuity equation in Lagrangian form can be written as:

$$\frac{\mathrm{d}\rho}{\mathrm{d}t} = -\rho\nabla\cdot\mathbf{v} \tag{7}$$

In SPH form, Eq. (7) can be written as:

$$\frac{\mathrm{d}\rho_a}{\mathrm{d}t} = \rho_a\sum_b \frac{m_b}{\rho_b}\mathbf{v}_{ab}\cdot\nabla_a W_{ab} \tag{8}$$

To avoid unphysical fluctuations in the pressure field, the continuity equation (including the density diffusion term) and the density diffusion term (Fourtakas et al., 2019) applied in the present study are given by:

$$\frac{\mathrm{d}\rho_a}{\mathrm{d}t} = \rho_a\sum_b \frac{m_b}{\rho_b}\mathbf{v}_{ab}\cdot\nabla_a W_{ab} + \delta h c_a\sum_b \frac{m_b}{\rho_b}\Psi_{ab}\cdot\nabla_a W_{ab} \tag{9}$$

$$\Psi_{ab} = 2\left(\rho_{ba}^T - \rho_{ab}^H\right)\frac{\mathbf{r}_{ab}}{|\mathbf{r}_{ab}|^2} \tag{10}$$

where δ is the free parameter which needs to be selected and the recommended value 0.1 is selected (Antuono et al., 2010) in the present work, superscript T and H denote the total and hydrostatic component respectively. In weakly compressible SPH (WCSPH), an equation of state is used to determine the fluid pressure based on the particle density. Tait's equation of state is widely used:

$$P = \frac{c_0^2\rho_0}{7}\left[\left(\frac{\rho}{\rho_0}\right)^7 - 1\right] \tag{11}$$

where ρ_0 is the reference density which equals to 1000 kg/m^3 and c_0 is the speed of sound at the reference density. In the present study however, the relationship between pressure and density is given by Morris' equation of state:

$$P = c_0^2(\rho - \rho_0) \tag{12}$$

Eq. (12) is used in several studies (Antuono et al., 2012; Sun et al., 2015) to reduce noise in the pressure field. The difference in the velocity when using Tait's equation of state for the focused wave test in this numerical wave-current flume is given in Appendix A. Particle positions are updated according to the following equation:

$$\frac{\mathrm{d}\mathbf{r}_a}{\mathrm{d}t} = \mathbf{v}_a \tag{13}$$

where $\mathbf{v}$ is velocity, $\mathbf{r}$ is position, t is time. Time stepping is given by the Symplectic method with time step criterion given a CFL value of 0.2 in the present study.

2.2. Modified dynamic boundary condition

The dynamic boundary condition (DBC) (Crespo et al., 2007) is the default boundary treatment in the DualSPHysics solver that enables complex geometries to be easily generated and provides efficient

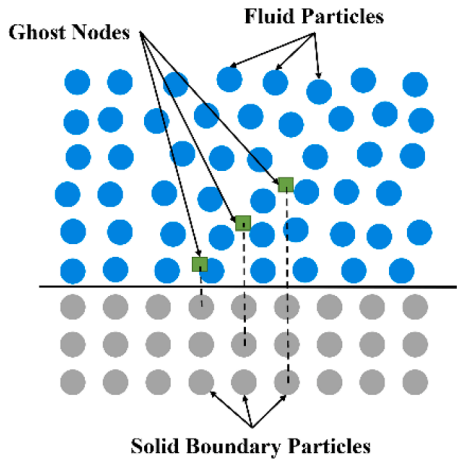

Fig. 1. General sketch of mirroring of ghost nodes for boundary particles, modified from English et al. (2022).

simulations. The boundary particles satisfy the same continuity equation as the fluid particles. The boundary particles remain fixed at their pre-defined locations with velocities set to zero to approximate the no-slip condition at the solid boundaries. The boundary particles can also move according to the imposed movement function, such as the wavemakers. However, the use of DBC presents a drawback where a gap between the fluid and the solid boundary is sometimes found due to the repulsive forces on the fluid particles. A modified dynamic boundary condition (mDBC) was presented in detail in English et al. (2022). The boundary particles are arranged in the same way as in DBC. A boundary interface is created between the fluid particles and the boundary particles. A ghost node for the boundary particle is projected into the fluid domain across the boundary interface similar to Marrone et al. (2011). The density of solid particles is obtained from positions of ghost nodes within the fluid domain by a linear extrapolation. A general sketch of the modified dynamic boundary condition is adapted from English et al. (2022) and shown in Fig. 1. The mDBC approximates a no-slip boundary condition with zero velocity applied to boundary particles at the bed. By using the mDBC, the unphysical gap between fluid and boundary commonly observed with the DBC is avoided and a more realistic local velocity variation achieved. The mDBC is applied herein.

2.3. Open boundary conditions

The wave generation by using a wavemaker and the wave absorption by using a damping zone or a dissipative beach are well developed for wave propagation simulations (Altomare et al., 2017). However, this is not appropriate when simulating a current where particles need to enter or leave the computational domain. Open boundaries are an alternative way to generate and absorb waves within DualSPHysics (Verbrugghe et al., 2019). The detailed implementation of open boundary conditions in DualSPHysics can be found in Tafuni et al. (2018). The algorithm is based on the use of the buffer zones which are defined near the inlet and the outlet of the computational domain. The physical quantities such as velocity, pressure and surface elevation can be imposed on the buffer particles or extrapolated from the fluid domain using ghost nodes. The imposed physical quantities can be obtained from theoretical solutions from wave theory, data from experiments and solutions from other numerical tools. For physical quantities extrapolated from the fluid domain using ghost nodes, the fluid quantities at ghost nodes are determined by the standard particle interpolation and then corrected to retrieve first order kernel and particle consistency by the method proposed by Liu and Liu (2006). A general sketch of the implemented open boundary is adapted from Tafuni et al. (2018) and shown in Fig. 2. The innermost dashed line represents the buffer threshold, followed by the buffer layers

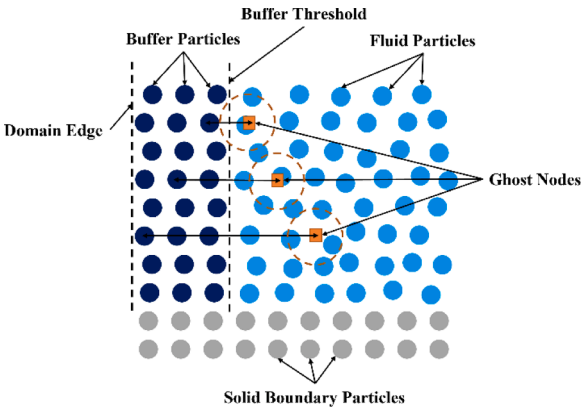

Fig. 2. General sketch of the implemented open boundary, modified from Tafuni et al. (2018).

of particles which are used to define the boundary condition. The positions of ghost nodes are determined by mirroring the particles into the fluid domain along the direction which is normal to the open boundary. The buffer width is selected to ensure full kernel support for the fluid particles near the inlet and the outlet.

3. Methodology for the numerical wave-current flume

3.1. General development of a numerical wave-current flume

A general sketch of a numerical wave flume using a piston-type wavemaker for wave generation and damping zone for wave absorption within DualSPHysics is shown in Fig. 3. Details of implementations can be found in Altomare et al. (2017). A general sketch of a numerical wave flume which uses open boundaries for wave generation and wave absorption within DualSPHysics is shown in Fig. 4. Details of implementations can be found in Verbrugghe et al. (2019). The two methods are available to build a numerical wave flume and are well tested within DualSPHysics.

In the present study, a numerical wave-current flume for wave-current conditions is developed based on the combination and modification of these two types of the numerical wave flume within DualSPHysics and a general sketch is shown in Fig. 5. Open boundaries are applied for generation of wave-alone, current-alone and wave-current conditions. Meanwhile, open boundaries are also applied for particles to leave or enter the fluid domain at both of the domain ends. A modified

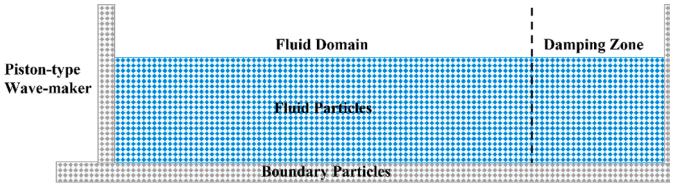

Fig. 3. General sketch of a numerical wave flume with the wavemaker and the damping zone.

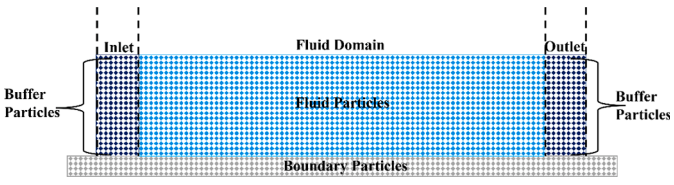

Fig. 4. General sketch of a numerical wave flume with open boundary conditions.

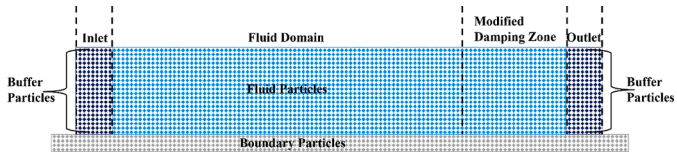

Fig. 5. General sketch of a numerical wave-current flume with open boundary conditions and modified damping zone.

damping zone described in more detail in Section 3.3, is applied at the end of the domain acting on the vertical orbital velocities enabling wave absorption with no interference on the current when a current exists. With this combination of open boundaries and a modified damping zone, a superposition of the current profile and current-altered wave-induced velocities is used for wave-current generation, whilst the current profile is introduced in the entire computational domain (at $t = 0$ s) and the outlet, and wave absorption is achieved simultaneously.

The numerical wave-current flume is easily implemented with the required physical quantities for the generation of wave-current conditions or waves-alone and current-alone test cases. Both following and opposing current conditions can be easily generated. Thus, the generation of regular, irregular, and focused waves in the presence of a current are readily achievable. Focused waves interacting with arbitrary sheared currents, representing complex and realistic wave-current conditions, can be achieved and are validated in the present study. In this numerical wave-current flume, accurate linear boundary conditions can be specified. Using focused waves allows for the accurate specification and generation of steep and breaking wave cases as long as the waves at the boundary are approximately linear (generally assumed for physical wave basins).

At both the inlet and the outlet, horizontal velocities and surface elevation are imposed and density is extrapolated from the fluid domain. According to Verbrugghe et al. (2019), no accuracy improvement can be gained by imposing vertical orbital velocities, but a negative impact on the particle spacing can occur. Similar observations are found in Ni et al. (2018). A sensitivity analysis was performed in Verbrugghe et al. (2019). It is suggested that at least 8 layers of buffer particles arranged in buffer zones can give accurate wave propagation simulations and this value is also used in the present study. The buffer zone at the inlet is divided into 3 vertical sections in the present study. A general sketch of the horizontal velocities imposing at the inlet is shown in Fig. 6 (a). In each vertical section, the horizontal velocities (time series) are imposed at 3 different heights. At each instant, the horizontal velocities at other heights in this section are given according to a parabolic fit function of DualSPHysics. A general sketch of one section of the buffer zone is shown in Fig. 6 (b). The accuracy of this approach is demonstrated later in Fig. 17.

3.2. Wave and wave-current generation

3.2.1. Regular, irregular and focused wave

For the generation of regular linear waves and regular non-linear waves using open boundary conditions in this numerical wave-current flume, the imposed physical quantities at the inlet are according to first-order and second-order Stokes wave theory respectively. To first-order, the surface elevation and the horizontal wave-induced velocities imposed at the inlet are given as:

$$\eta(t) = a\cos(kx - \omega t + \varphi) \tag{14}$$

$$v_x(z,t) = \frac{gak}{\omega}\frac{\cosh(k(z+d))}{\cosh(kd)}\cos(kx - \omega t + \varphi) \tag{15}$$

where g is the acceleration due to gravity, d is the water depth, a is the wave amplitude, ω is the angular frequency, k is the wavenumber, φ is the initial phase (at $x = 0$ and $t = 0$). To second-order, the surface elevation and the horizontal wave-induced velocities imposed at the inlet are given as:

$$\eta(t) = \frac{H}{2}\cos(kx - \omega t + \varphi) + \frac{\pi H^2}{8L}\frac{\cosh(kd)}{\sinh^3(kd)}(2 + \cosh(2kd))\cos(2(kx - \omega t + \varphi)) \tag{16}$$

$$v_x(z,t) = \frac{\pi H}{T}\frac{\cosh(k(z+d))}{\sinh(kd)}\cos(kx - \omega t + \varphi) + \frac{3}{4}\frac{\pi H}{T}\frac{\pi H}{L}\frac{\cosh(2k(z+d))}{\sinh^4(kd)}\cos(2(kx - \omega t + \varphi)) \tag{17}$$

where H is the wave height, L is the wavelength, T is the wave period. For the generation of irregular waves, the Pierson-Moskowitz spectrum or the JONSWAP spectrum (Hasselmann et al., 1973) with the specified parameters can be selected. With the selected frequency interval, Δf, the spectrum is then uniformly divided, and for each frequency f_i a linear wave component is defined. For each value of angular frequency ω_i ($\omega_i = 2\pi f_i$), the wavelength L_i and the wavenumber k_i ($k_i = 2\pi/L_i$) is solved using the standard linear dispersion relation:

$$\omega_i^2 = gk_i\tanh(k_i d) \tag{18}$$

The initial phase φ_i of each linear wave is assigned a random number uniformly distributed between 0 and 2π. The amplitude a_i of each wave component can be determined by the following equation, where $S_i(f)$ is calculated based on the selected wave spectrum.

$$a_i = \sqrt{2S_i(f)\Delta f} \tag{19}$$

A focused wave group is often used to approximate the extreme wave

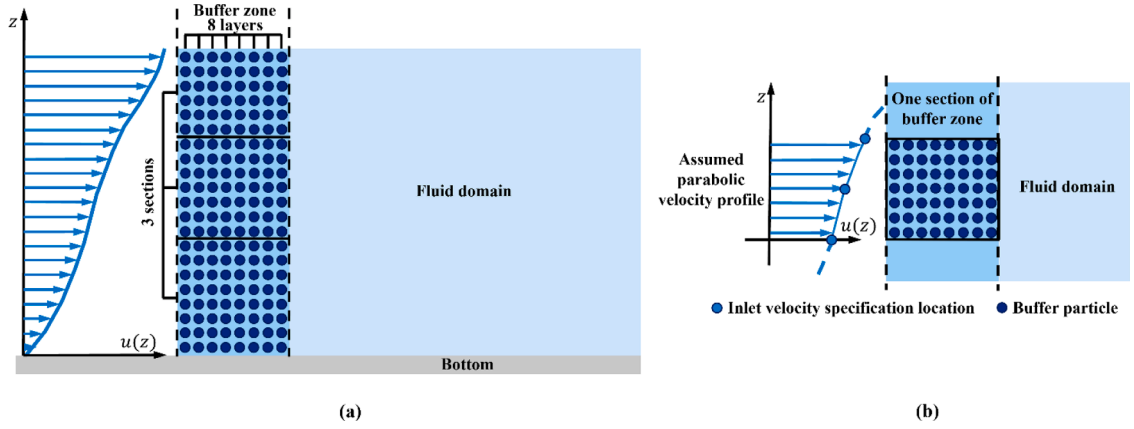

Fig. 6. General sketch of (a) the horizontal velocities imposing at the inlet, (b) one section of the buffer zone at the inlet.

conditions in offshore and ocean engineering. The focused wave group is composed of a number of individual wave components. If the focused wave is achieved at the focal time t_f and the focal location x_f, the initial phase of each wave component is obtained according to:

$$\varphi_i = -k_i x_f + \omega_i t_f \tag{20}$$

where π can be an addition into Eq. (20) for generation of a trough-focused wave. In the focused wave group, the amplitude of each wave component can be determined in terms of the wave spectrum $S_i(f)$ and the focused amplitude A_f:

$$a_i = \frac{A_f S_i(f)\Delta f}{\sum_{l=1}^{N} S_l(f)\Delta f} \tag{21}$$

The imposed surface elevation and horizontal wave-induced velocity of the irregular wave and the focused wave at the inlet are given by:

$$\eta(t) = \sum_{i=1}^{N} a_i \cos(k_i x - \omega_i t + \varphi_i) \tag{22}$$

$$v_x(z,t) = \sum_{i=1}^{N} \frac{g a_i k_i}{\omega_i} \frac{\cosh(k_i(z+d))}{\cosh(k_i d)} \cos(k_i x - \omega_i t + \varphi_i) \tag{23}$$

where φ_i is a random number between 0 and 2π for generation of an irregular wave group and is calculated according to Eq. (20) for generation of a focused wave group, a_i is calculated according to Eq. (19) for generation of an irregular wave group and is calculated according to Eq. (21) for generation of a focused wave group.

3.2.2. Wave interacting with uniform and linearly sheared current

The wavelengths are altered when interacting with a current. The relationship between the wavelength and the frequency no longer satisfies the standard linear dispersion relation without the Doppler shift in Eq. (18). For a steady and uniform current, a modified dispersion relation is proposed in Jonsson (1990) as follows:

$$(\omega - kU_c)^2 = gk\tanh(kd) \tag{24}$$

where g is the acceleration due to gravity, d is the water depth, k is the current modified wavenumber, ω is the angular frequency, $\omega_r = \sqrt{gk\tanh(kd)}$ is the relative angular frequency, $U_c = U_s$ is the uniform current velocity which is defined as positive for waves in a following current and negative in an opposing current. U_s is the surface current. For a linear wave interacting with a linearly sheared current with constant vorticity across the water depth, the modified dispersion relation is (Nwogu, 2009):

$$(\omega - kU_s)^2 = (gk - \Omega_s(\omega - kU_s))\tanh(kd) \tag{25}$$

where U_s is the surface current, Ω_s is the constant vorticity equal to U_s/d, the linearly sheared current is defined as $U_c(z) = U_s + \Omega_s z$. The current modified wavenumber k can be obtained from Eqs. (24) and (25) for a linear wave interacting with the uniform current and the linearly sheared current respectively. In the flume where waves propagate from a zero-current region to a region with current (e.g. a current inlet), there must be consideration of the amplitude modification by the current when defining boundary conditions in order to obtain the desired wave-current conditions. This is not required for the open boundary approach in the present numerical wave-current flume which is capable of the precise specification of the combined wave-current conditions together. Therefore, the individual wave amplitude is obtained in the same way as described in Section 3.2.1. With the current modified wavenumber k, the wave amplitude a, and the angular frequency ω, the surface elevation and the total horizontal particle velocity imposed at the inlet for an individual linear wave interacting with the current are given by:

$$\eta(t) = a\cos(kx - \omega t + \varphi) \tag{26}$$

$$\begin{aligned} v_x(z,t) &= U_c(z) + U_w(z,t) \\ &= U_c(z) + a(\omega - kU_s)\frac{\cosh(k(z+d))}{\sinh(kd)}\cos(kx - \omega t + \varphi) \end{aligned} \tag{27}$$

where $U_w(z,t)$ is the wave-induced velocity and $U_c(z)$ is the velocity due to the current. For Eq. (27), details can be found in Silva et al. (2016) and Chen and Basu (2019). $U_c(z)$ is also applied at the outlet. Similarly, to generate the irregular wave group and the focused wave group consisting of linear wave components interacting with the uniform or the linearly sheared current, the surface elevation and the total horizontal particle velocity imposed at the inlet are given by:

$$\eta(t) = \sum_{i=1}^{N} a_i \cos(k_i x - \omega_i t + \varphi_i) \tag{28}$$

$$\begin{aligned} v_x(z,t) &= U_c(z) + U_w(z,t) \\ &= U_c(z) + \sum_{i=1}^{N} a_i(\omega_i - k_i U_s)\frac{\cosh(k_i(z+d))}{\sinh(k_i d)}\cos(k_i x - \omega_i t + \varphi_i) \end{aligned} \tag{29}$$

where φ_i is a random number between 0 and 2π for the generation of an irregular wave group. For the generation of a focused wave group, φ_i is calculated according to Eq. (20), but using the current modified wavenumber obtained by the modified dispersion relation.

3.2.3. Wave interacting with arbitrary sheared current

In the study of Li and Ellingsen (2019), a direct integration method (DIM) was presented which can numerically evaluate the dispersion relation of a linear surface wave interacting with arbitrary sheared current. For this purpose, it is argued that the DIM is superior to the two existing numerical methods, the piecewise linear approximation method (e.g., Zhang, 2005) and the method described in Dong and Kirby (2012). The DIM is implemented in an iterative procedure with standard constituent methods and combines only standard operations for solving linear inhomogeneous differential equations, numerical integration, and root finding (Li and Ellingsen, 2019). The detailed descriptions of the method can refer to Li and Ellingsen (2019). One of the main advantages is that it is easy (and computationally efficient) to compute the full linear wave-induced velocities, which is required for the definition of the inlet boundary condition.

With the modified wavenumber and the modified wave-induced kinematics obtained, linear waves interacting with arbitrary sheared current can be generated. In the present study, a current profile defined according to the power law method will be selected to represent the arbitrary sheared current for validation of the numerical wave-current flume which is given by:

$$U_c(z) = U_s\left(\frac{z+d}{d}\right)^n \tag{30}$$

where U_s is the surface current, n is equal to 1/3 in the present study.

3.3. Wave absorption

The use of a wave absorption method to avoid wave reflection can be achieved by either a dissipative beach or a damping zone arranged at the end of the domain. A dissipative beach consists of the solid boundary closing the domain end with no access for particles entering or leaving the fluid domain required to maintain a current field. Therefore, a damping zone which is arranged near the outlet open boundary instead of the solid boundary wall will be an appropriate solution for wave absorption in the present study. However, the damping zone should be modified to be applied only to the vertical velocity component when simulating wave-current interactions to avoid interference on the current. A similar approach was applied in Zhang et al. (2014). In DualSPHysics, the velocity is reduced in the damping zone according to the

following equations:

$$\mathbf{v} = \mathbf{v}_0 \cdot f(x, \Delta t) \tag{31}$$

$$f(x, \Delta t) = 1 - \Delta t \cdot \beta \cdot \left(\frac{x - x_0}{x_1 - x_0}\right)^2 \tag{32}$$

where $\mathbf{v}_0$ is the initial velocity of the particle, $\mathbf{v}$ is the final velocity of the particle, $f(x, \Delta t)$ is the reduction function, Δt is the duration of the last time step, x is the position of particles, x_0 and x_1 are the initial and the final position of the damping zone respectively, β is the coefficient to modify the reduction function. In the present study, both horizontal velocity component and vertical velocity component are reduced to absorb waves for linear wave-only cases with $\beta = 10$. When a current exists, only the vertical velocity component is reduced to absorb waves with $\beta = 300$ for the second-order Stokes wave test considering the Stokes drift current and the wave-current interaction tests. This value of β (= 300) provides a relatively quick reduction in velocity and has good absorption performance.

4. Wave-alone and current-alone tests

The implementation of generating wave-current conditions in this numerical wave-current flume is initially validated with theoretical results for wave-alone tests and current-alone tests in this section. The wave-alone tests consist of a second-order Stokes wave, linear irregular wave and focused wave whilst the current-alone tests consist of a uniform current, a linearly sheared current and an arbitrary sheared current defined by a power law profile as an example. The test cases are listed in Table 1. For the second column in the table, 0.15 m is the wave height for the regular wave, 0.1 m is the significant wave height for the irregular waves, and 0.05 m is the focused amplitude for the focused wave. For the wave period column, 2 s is the wave period for regular wave, and 2 s and 3 s are the peak period for the irregular wave and the focused wave respectively. The JONSWAP spectrum with peak enhancement factor $\gamma = 3.3$ is used for the irregular wave test and the focused wave test. For the water depths, 0.66 m is selected for the regular wave test as used in Altomare et al. (2017), 1.5 m is selected for the other tests. 0.1 m/s is the uniform current speed, and 0.15 m/s and 0.09 m/s are the surface currents of linearly sheared current and arbitrary sheared current. For simulations of the regular wave and the irregular wave, the domain length is 12 m and the damping zone length is 6 m. For simulation of the focused wave, the domain length is 11 m and the damping zone length is 11 m. The damping zone length used in the focused wave test is set according to the peak wavelength L_p such that $L_{damping}/L_p \approx 1.1$. A difference in using a damping zone ($L_{damping} = 6$ m) for the focused wave test in this numerical wave-current flume is given in Appendix A.

The setup of the numerical wave-current flume is shown in Fig. 7. WG is the wave gauge location where the numerical free-surface elevations are measured and compared with the theoretical solutions. VG is the location where numerical velocities are measured and compared with the theoretical solutions. WG and VG are locations just for time-domain comparisons. Additional measurement locations are arranged for spatial comparison for the focused wave test and the wave-current interaction tests. Measurement locations for the surface elevation profile and the velocity profile are given in Section 4.2 and Section 5. The wave generation method is described in Section 3.2.1. The wave tests are compared with theoretical surface elevations and orbital velocities, and the current tests are compared with target mean vertical profiles.

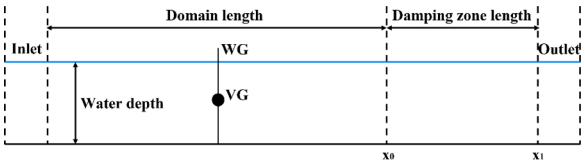

Fig. 7. Setup of the numerical wave-current flume (WG denotes wave gauge, VG denotes velocity gauge).

4.1. Regular wave and irregular wave

In order to check the regular wave and the irregular wave generation in this numerical wave-current flume, regular waves and irregular waves are simulated in a numerical flume with a domain length (L_{domain}) equal to 12 m ($L_{domain}/L \approx 2.7$ for the regular wave, $L_{domain}/L_p \approx 2.1$ for the irregular wave, the peak wavelength L_p) and a damping zone length ($L_{damping}$) equal to 6 m. The wavelength of the regular wave is 4.52 m, and the peak wavelength of the irregular waves is 5.78 m. The damping zone requires approximately 33% of the total runtime. The numerical surface elevations are measured in the middle of the domain, whilst the numerical horizontal and vertical orbital velocities are also measured in the middle of the domain (z/d = -0.5 for the regular wave and z/d = -1/3 for the irregular wave). The measured numerical results for the regular wave and the irregular wave are compared with the theoretical solutions in Figs. 8 and 9 respectively.

As shown in the figures, a high accuracy in simulating the regular wave and the irregular waves in this numerical wave-current flume is achieved. In order to quantify the accuracy of the simulations, RMSE value over time for the surface elevations (e.g. from $t = t_1$ $(i = 1)$ to $t = t_n$ $(i = n)$) for a fixed location x is calculated as follows:

$$RMSE(\eta(x)) = \frac{1}{\max_i\left(\eta(x, t_i)^{theory}\right)} \sqrt{\frac{1}{n}\sum_{i=1}^{n}\left(\eta(x, t_i)^{measured} - \eta(x, t_i)^{theory}\right)^2} \tag{33}$$

The non-dimensional RMSE values are listed in Table 2. The RMSE values are 9.3% for the regular wave (based on a 30 s time duration from 30 s to 60 s, the measured numerical results becoming stable after the initial stage at around 6 s) and 7.7% for the irregular wave (based on a 30 s time duration from 10 s to 40 s, the measured numerical results becoming stable after the initial stage at around 7 s).

4.2. Focused wave

In this section, the focused wave simulation is validated to check the accuracy of the numerical wave-current flume. The focused wave is simulated in a numerical flume with a domain length (L_{domain}) equal to

Table 1
Test cases.

Test number	Wave height H, significant wave height H_s, or focused amplitude A_f [m]	Wave period T or peak period T_p [s]	Water depth d [m]	Surface current U_s [m/s]	Domain length L_{domain} [m]	Damping zone length $L_{damping}$ [m]	Test duration t [s]
1. Regular wave	0.15	2	0.66	/	12	6	60
2. Irregular wave	0.1	2	1.5	/	12	6	40
3. Focused wave	0.05	3	1.5	/	11	11	32
4. Uniform current	/	/	1.5	±0.1	11	/	32
5. Linearly sheared current	/	/	1.5	±0.15	11	/	32
6. Arbitrary sheared current	/	/	1.5	±0.09	11	/	32

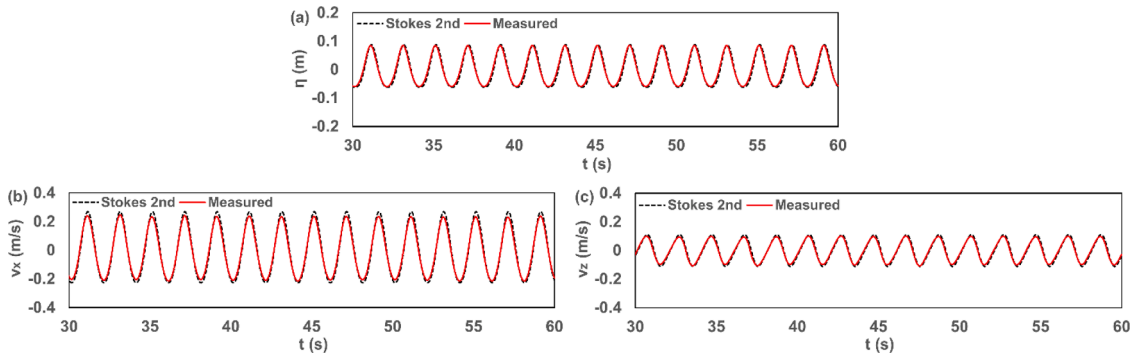

Fig. 8. Comparison between theoretical and numerical results for the regular wave (a) surface elevation at $x = 6.0$ m, (b) horizontal velocity at $x = 6.0$ m, $z/d = -0.5$, (c) vertical velocity at $x = 6.0$ m, $z/d = -0.5$.

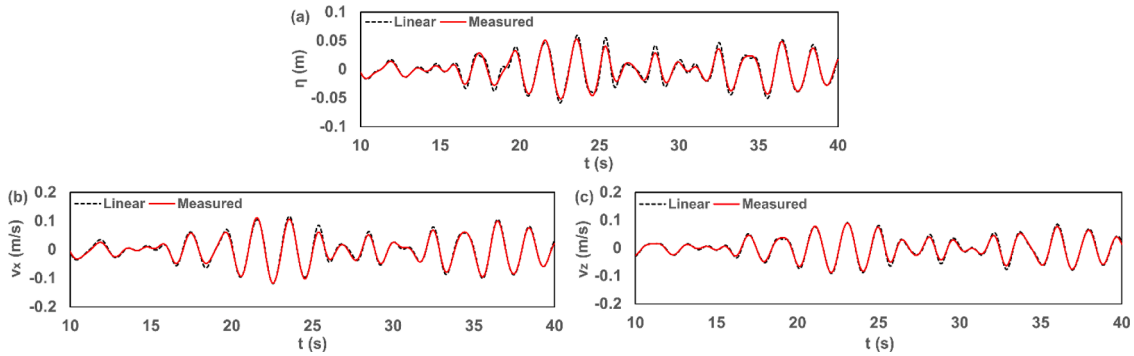

Fig. 9. Comparison between theoretical and numerical results for the irregular wave (a) surface elevation at $x = 6.0$ m, (b) horizontal velocity at $x = 6.0$ m, $z/d = -1/3$, (c) vertical velocity at $x = 6.0$ m, $z/d = -1/3$.

Table 2
RMSE values of the regular wave and the irregular wave tests.

	Regular wave	Irregular wave
$RMSE(\eta(x))$	0.093	0.077

11 m ($L_{domain}/L_p \approx 1.1$, the peak wavelength L_p) and a damping zone length ($L_{damping}$) equal to 11 m. The focused wave is achieved at the focal time $t_f = 16$ s and the focal location $x_f = 5.5$ m which is the centre of the domain. An increase of domain length means more particles with increased computational time. If a high accuracy can be achieved with a shorter domain length, it will benefit simulation efficiency. For the focused wave test case, the surface elevations are measured in the middle of the domain, while the orbital velocities are also measured in the middle of the domain at VG ($z/d = -1/3$). Meanwhile, the surface elevation profile is measured at the focal time from 0.2 m to 10.8 m in the fluid domain. At the focal location, the horizontal orbital velocity profile at the focal time and the vertical orbital velocity profile at 15.5 s (where these values are close to be at a maximum) are selected for the comparison with the theoretical results. The measured numerical results for the focused wave are compared with the theoretical solutions in Fig. 10. The horizontal velocity field at the focal time for the simulation (damping zone is included) is shown in Fig. 11.

The RMSE value for the surface elevation (time series) is calculated based on Eq. (33) and RMSE value over depth for the velocities (e.g. from $z = z_1$ $(j = 1)$ to $z = z_n$ $(j = n)$) for a fixed time t is calculated as follows:

$$RMSE(v_x(t)) = \frac{1}{\max_{j,t}\left(\left|v_x(z_j,t)^{theory}\right|\right)}\sqrt{\frac{1}{n}\sum_{j=1}^{n}\left(v_x(z_j,t)^{measured} - v_x(z_j,t)^{theory}\right)^2} \tag{34}$$

$$RMSE(v_z(t)) = \frac{1}{\max_{j,t}\left(\left|v_z(z_j,t)^{theory}\right|\right)}\sqrt{\frac{1}{n}\sum_{j=1}^{n}\left(v_z(z_j,t)^{measured} - v_z(z_j,t)^{theory}\right)^2} \tag{35}$$

Note that the RMSE values computed for time t are normalized by the maximum value over all time. The non-dimensional RMSE values are listed in Table 3. The RMSE value is 3.3% for the surface elevation (based on a time duration from 10 s to 22 s based on $t_f \pm 2T_p$), 2.1% for the horizontal orbital velocity and 2.6% for the vertical orbital velocity which demonstrates high accuracy of the focused wave simulation in the wave-current flume.

4.3. Convergence study

The particle size (0.02 m) used in the simulations in Section 4 has been shown to provide accurate results for tests of the regular wave, the irregular wave and the focused wave. However, a convergence study has been carried out for the focused wave simulation with different initial interparticle distances referred to as particle sizes (d_p) herein since the focused wave is used for the simulations of the wave-current interactions in the next section. Three particle sizes (0.06 m, 0.05 m and 0.02 m) were selected in the convergence study due to an integer value of the ratio d/d_p is recommended (Altomare et al., 2017). The time series of the free-surface elevation for each particle size is shown in Fig. 12. As d_p reduces, the agreement with theory improves.

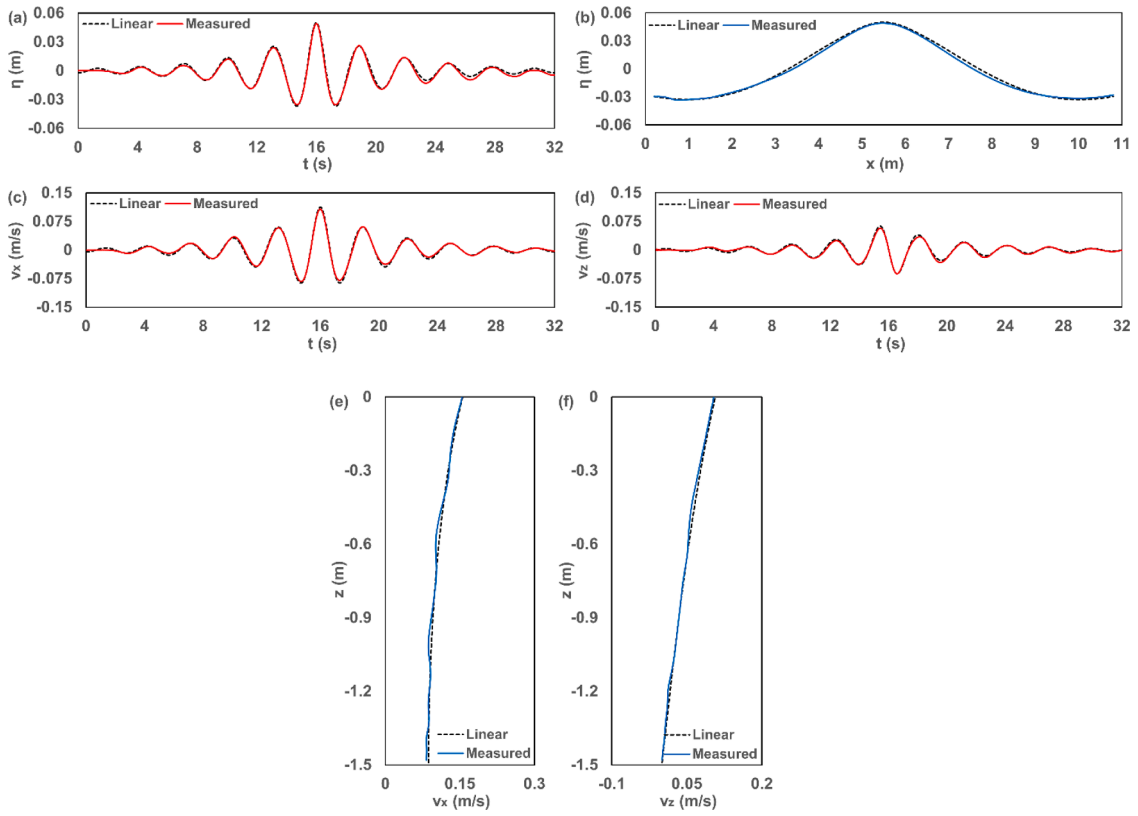

Fig. 10. Comparison between theoretical and numerical results for the focused wave (a) surface elevation at $x = 5.5$ m, (b) surface elevation profile at $t = 16$ s, (c) horizontal velocity at $x = 5.5$ m, $z/d = -1/3$, (d) vertical velocity at $x = 5.5$ m, $z/d = -1/3$, (e) horizontal velocity profile at $t = 16$ s, (f) vertical velocity profile at $t = 15.5$ s.

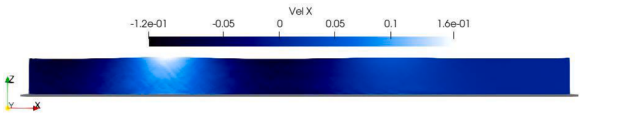

Fig. 11. Instant (the focal time) of the horizontal velocity field for the focused wave.

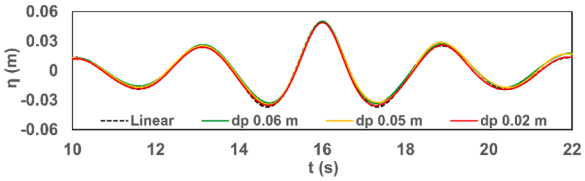

Fig. 12. Surface elevation for different particle sizes in the focused wave test.

Table 3
RMSE values of the focused wave test.

	Focused wave
$RMSE(\eta(x))$	0.033
$RMSE(v_x(t))$	0.021
$RMSE(v_z(t))$	0.026

Table 4
RMSE values, runtimes and number of particles with different resolutions of the focused wave test.

	dp [m]	$RMSE(\eta(x))$	*Runtime* [h]	Np [10^4]
particle size 1	0.06	0.040	0.253	1.09
particle size 2	0.05	0.039	0.290	1.54
particle size 3	0.02	0.033	1.896	8.86

The non-dimensional RMSE values (time series of surface elevation) is calculated based on Eq. (33). According to the RMSE values for the surface elevation (based on a time duration from 10 s to 22 s), runtime and total number of particles (N_p) listed in Table 4, using the resolution (0.02 m) improves the accuracy of the simulation compared with the resolution (0.05 m) with RMSE value decreasing from 0.039 to 0.033 (an approximately 6.5 times bigger runtime and an even finer resolution means an even longer runtime, computed on an Nvidia GeForce GTX 950M GPU). Therefore, the particle size 0.02 m was selected for all simulations herein.

4.4. Current

In this section, the current-alone tests are simulated. The current profiles are listed in Table 1. The same current profiles will be applied in the Section 5 for wave-current interaction tests. In the middle of the domain, the average velocity profiles during the entire simulation (0 s to 32 s) with error bars showing the standard deviations for different depths are compared with the target ones in Fig. 13. As shown in the figure, the profiles of the uniform current, the linearly sheared current and the arbitrary sheared current defined by a power law profile in both

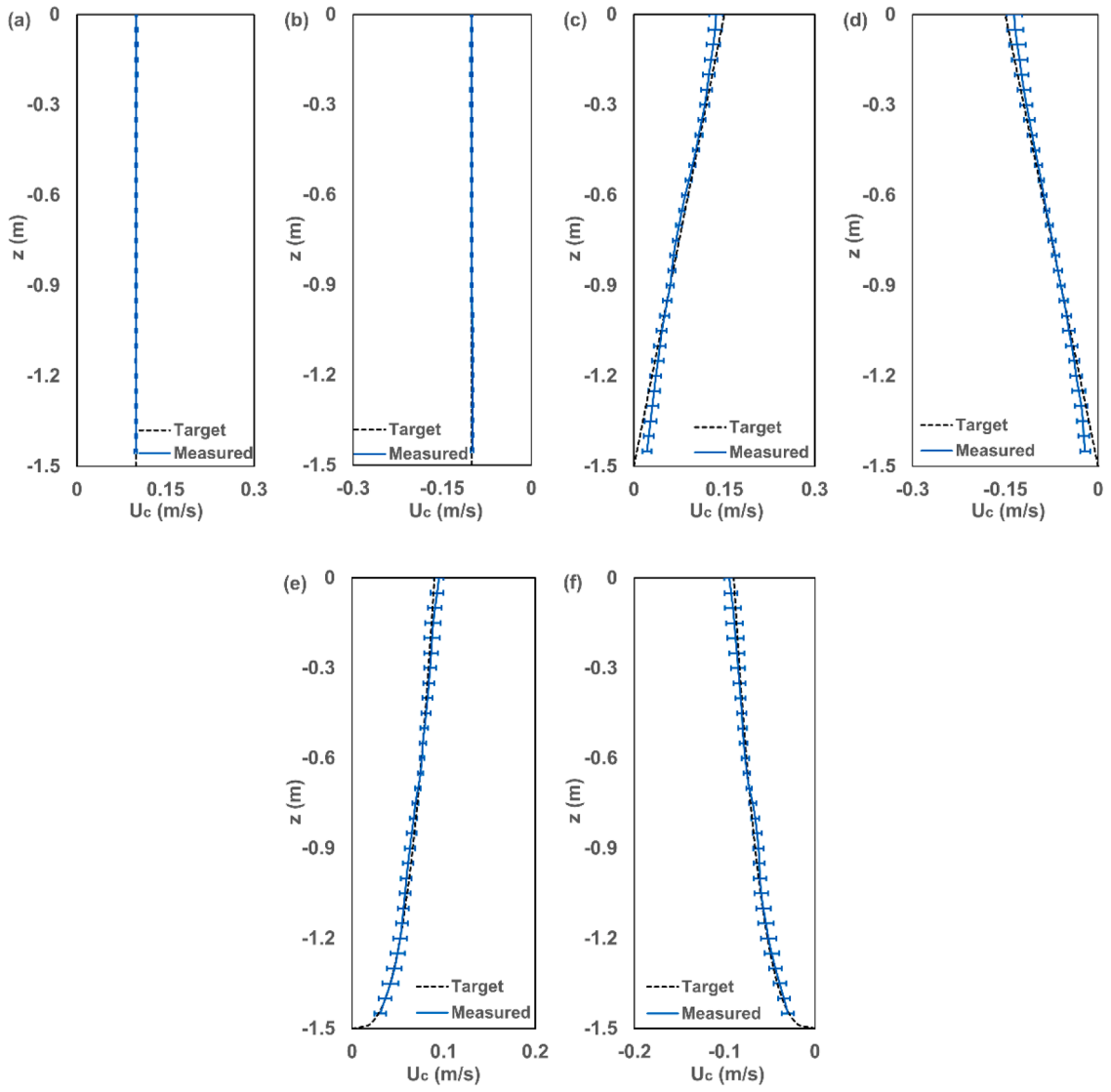

Fig. 13. The average velocity profile of the currents with error bars showing the standard deviations for different depths (a) following uniform current, (b) opposing uniform current, (c) following linearly sheared current, (d) opposing linearly sheared current, (e) following arbitrary sheared current, (f) opposing arbitrary sheared current.

following and opposing directions are acceptable. Taking the following arbitrary sheared current of test number 6 as an example, the average velocity profiles at different times (from 0 s to 8 s, from 8 s to 16 s, from 16 s to 24 s and from 24 s to 32 s) in the middle of the domain are compared with the target one in Fig. 14 and the average velocity profiles during the entire simulation (0 s to 32 s) in different sections of the

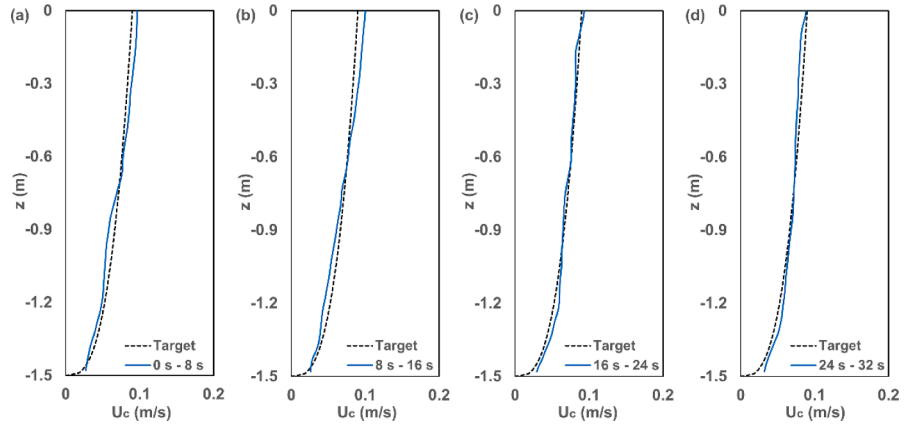

Fig. 14. The average velocity profile of the following arbitrary sheared current at different times in the middle of the domain (a) from 0 s to 8 s, (b) from 8 s to 16 s, (c) from 16 s to 24 s, (d) from 24 s to 32 s.

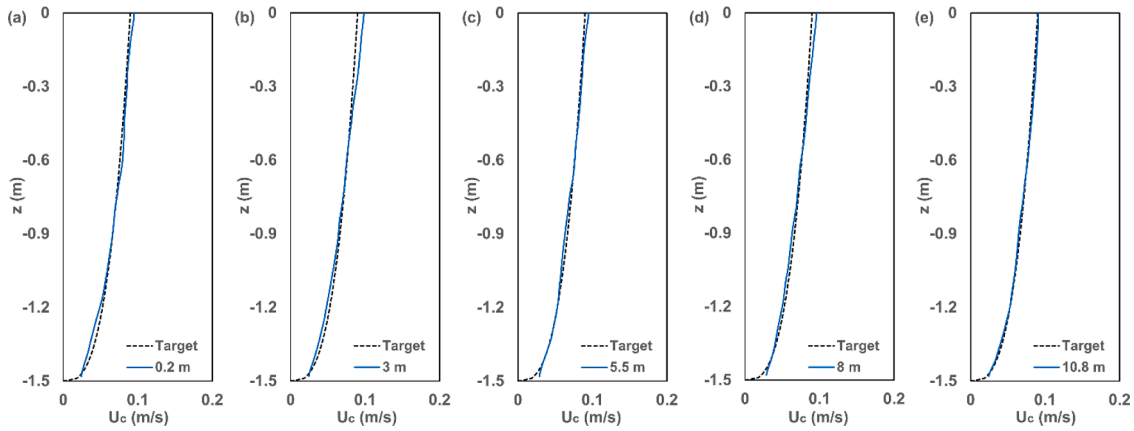

Fig. 15. The average velocity profile of the following arbitrary sheared current during the entire simulation in different sections of the domain (a) $x = 0.2$ m, (b) $x = 3$ m, (c) $x = 5.5$ m, (d) $x = 8$ m, (e) $x = 10.8$ m.

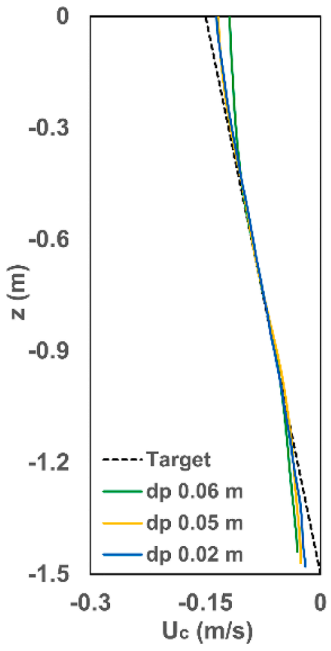

Fig. 16. The average velocity profile for different particle sizes in the opposing linearly sheared current test.

domain (0.2 m near the inlet, 3 m, 5.5 m, 8 m and 10.8 m near the outlet) are compared with the target one in Fig. 15. The particle size (0.02 m) has been shown to provide accurate results for tests of the currents. However, a convergence study has been carried out for the linearly sheared current in opposing direction with three different particle sizes. In the middle of the domain, the average velocity profiles during the entire simulation (0 s to 32 s) are shown in Fig. 16. It is evident that the results from the coarse resolutions (0.06 m and 0.05 m) are less accurate than the result from a finer resolution (0.02 m). The particle size 0.02 m was used.

5. Wave-current interaction tests

The implementation of the numerical wave-current flume to generate wave-current conditions is validated in this section. The focused wave interacting with the uniform current, the linearly sheared current and the arbitrary sheared current defined by a power law profile respectively represent the complex wave-current conditions. The test cases are listed in Table 5. The JONSWAP spectrum with peak enhancement factor $\gamma = 3.3$ is used for the wave-current interaction tests. For all the simulations, the numerical flume has a domain length equal to 11 m and a damping zone length equal to 11 m that is the same with the numerical flume in Section 4.2. For all test cases, the surface elevations are measured in the middle of the domain, while the velocities are also measured in the middle of the domain at VG ($z/d = -1/3$). The focused wave in a current is achieved at the focal time $t_f = 16$ s and the focal location $x_f = 5.5$ m which is the centre of the domain. The surface elevation profile is measured at the focal time from 0.2 m to 10.8 m in the fluid domain. At the focal location, the horizontal velocity profile at the focal time and the vertical velocity profile at 15.5 s (where these values are close to maximum) are selected for the comparison with the theoretical results. The generation methods of wave-current conditions are described in Section 3.2.2 and Section 3.2.3. The numerical results are compared with theoretical solutions in terms of surface elevations and velocities. For test number 3, 7, 8, 9, 10, 11, and 12, the measured horizontal velocity profiles at the inlet are compared with theoretical solutions at 0 s and 14.25 s (where these values are close to maximum) in Fig. 17 which indicates that the generation method described in Section 3.1 is accurate.

Table 5
Test cases.

Test number	Focused amplitude A_f [m]	Peak period T_p [s]	Water depth d [m]	Surface current U_s [m/s]	Domain length L_{domain} [m]	Damping zone length $L_{damping}$ [m]	Test duration t [s]
7. Focused wave - Uniform current (following)	0.05	3	1.5	0.1	11	11	32
8. Focused wave - Uniform current (opposing)	0.05	3	1.5	-0.1	11	11	32
9. Focused wave - Linearly sheared current (following)	0.05	3	1.5	0.15	11	11	32
10. Focused wave - Linearly sheared current (opposing)	0.05	3	1.5	-0.15	11	11	32
11. Focused wave - Arbitrary sheared current (following)	0.05	3	1.5	0.09	11	11	32
12. Focused wave - Arbitrary sheared current (opposing)	0.05	3	1.5	-0.09	11	11	32

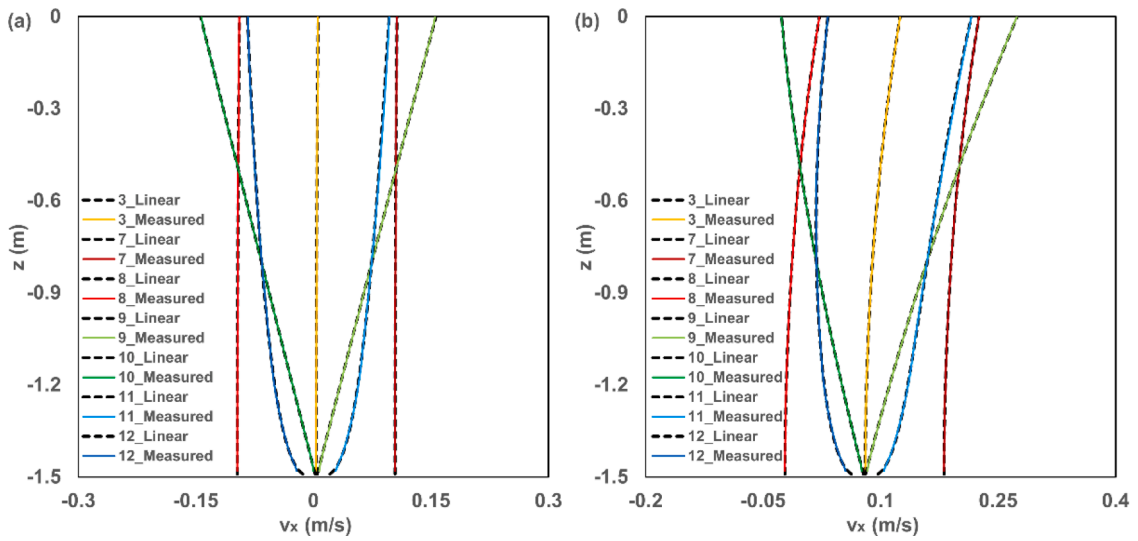

Fig. 17. Comparison between the measured horizontal velocity profiles and theoretical solutions at the inlet (a) horizontal velocity profile at $t = 0$ s, (b) horizontal velocity profile at $t = 14.25$ s.

5.1. *Focused wave interacting with uniform current*

The results of the focused wave interacting with a following uniform current and an opposing uniform current are compared with the theoretical solutions. The measured numerical results are compared with the theoretical solutions in Fig. 18 for the focused wave in the following uniform current and in Fig. 19 for the focused wave in the opposing uniform current.

The non-dimensional RMSE values (time series of surface elevation and profile of velocity) calculated based on Eqs. (33) - (35) are listed in Table 6. The RMSE values for the surface elevation are 4.5% and 4.1% in the following and opposing current respectively (based on a time duration from 10 s to 22 s). The RMSE values range from 1.2% to 2.6% for the velocities. The RMSE values demonstrate high accuracy of the generation of waves interacting with a uniform current in both following and opposing directions.

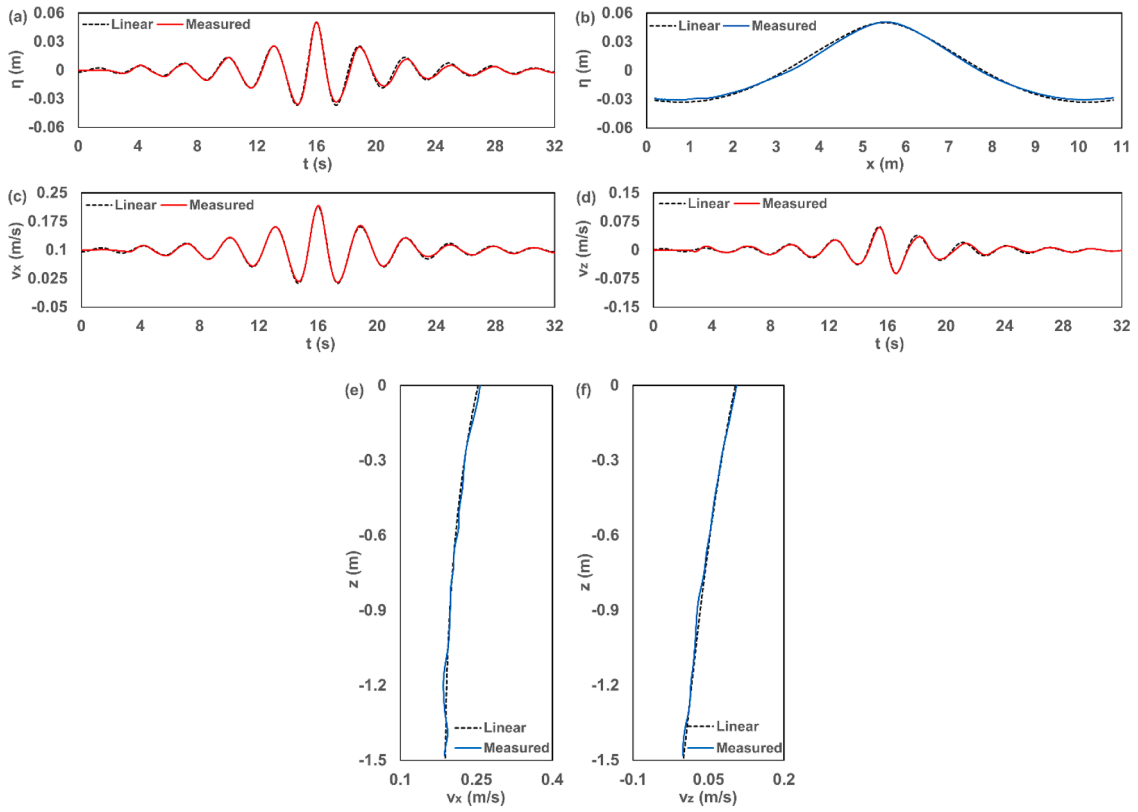

Fig. 18. Comparison between theoretical and numerical results for the focused wave interacting with the following uniform current (a) surface elevation at $x = 5.5$ m, (b) surface elevation profile at $t = 16$ s, (c) horizontal velocity at $x = 5.5$ m, $z/d = -1/3$, (d) vertical velocity at $x = 5.5$ m, $z/d = -1/3$, (e) horizontal velocity profile at $t = 16$ s, (f) vertical velocity profile at $t = 15.5$ s.

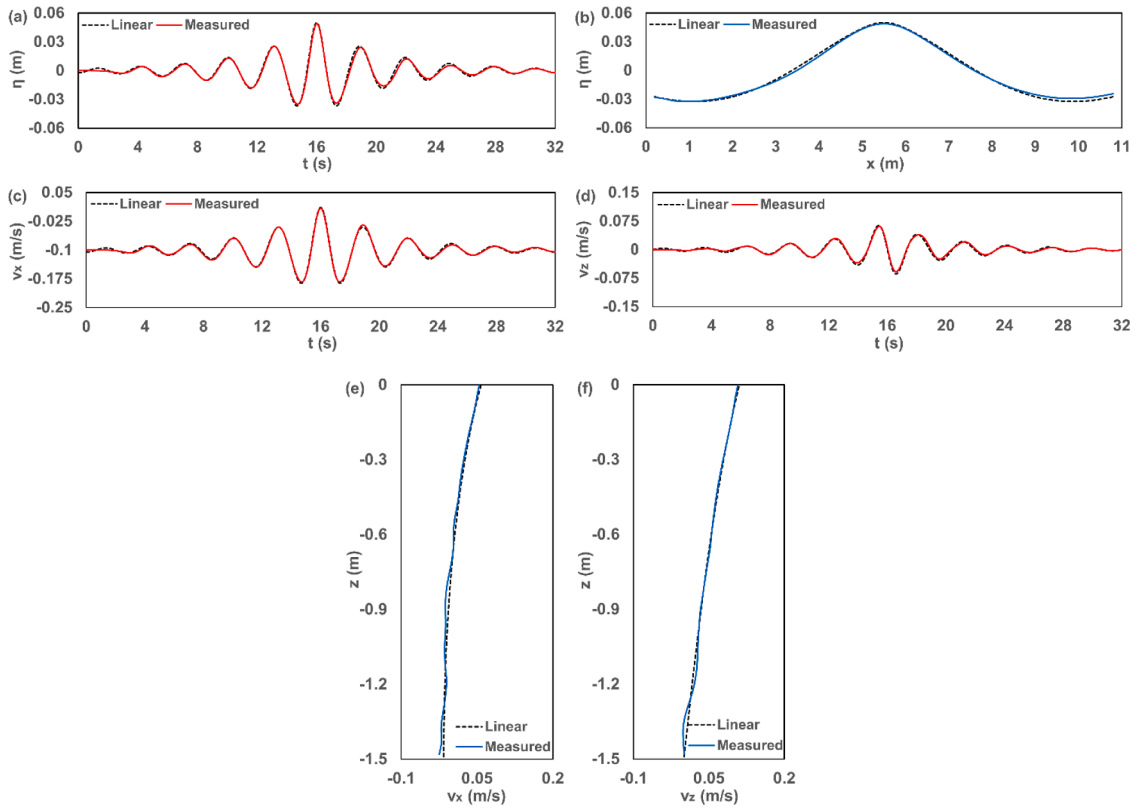

Fig. 19. Comparison between theoretical and numerical results for the focused wave interacting with the opposing uniform current (a) surface elevation at $x = 5.5$ m, (b) surface elevation profile at $t = 16$ s, (c) horizontal velocity at $x = 5.5$ m, $z/d = -1/3$, (d) vertical velocity at $x = 5.5$ m, $z/d = -1/3$, (e) horizontal velocity profile at $t = 16$ s, (f) vertical velocity profile at $t = 15.5$ s.

Table 6
RMSE values of the focused wave interacting with the uniform current.

	Focused wave in the following current	Focused wave in the opposing current
$RMSE(\eta(x))$	0.045	0.041
$RMSE(v_x(t))$	0.012	0.016
$RMSE(v_z(t))$	0.025	0.026

5.2. Focused wave interacting with linearly sheared current

The results of the focused wave interacting with a following linearly sheared current and an opposing linearly sheared current are compared with the theoretical solutions. The measured numerical results are compared with the theoretical solutions in Fig. 20 for the focused wave in the following linearly sheared current and in Fig. 21 for the focused wave in the opposing linearly sheared current.

The non-dimensional RMSE values (time series of surface elevation and profile of velocity) calculated based on Eqs. (33) - (35) are listed in Table 7. The RMSE values for the surface elevation are 5.6% and 4.7% in the following and opposing current respectively (based on a time duration from 10 s to 22 s). The RMSE values range from 3.0% to 5.5% for the velocities. The RMSE values are higher for the sheared cases due to the temporal variability and that the linearly sheared current profiles are not exactly as assumed in the theory. The RMSE values demonstrate good accuracy for the simulation of waves interacting with a linearly sheared current in both following and opposing directions.

5.3. Focused wave interacting with arbitrary sheared current

The results of the focused wave interacting with a following arbitrary sheared current and an opposing arbitrary sheared current are compared with the theoretical solutions. The measured numerical results are compared with the theoretical solutions in Fig. 22 for the focused wave in the following arbitrary sheared current and in Fig. 23 for the focused wave in the opposing arbitrary sheared current.

The non-dimensional RMSE values (time series of surface elevation and profile of velocity) calculated based on Eqs. (33) - (35) are listed in Table 8. The RMSE values for the surface elevation are 4.9% and 5.4% in the following and opposing current respectively (based on a time duration from 10 s to 22 s). The RMSE values range from 2.0% to 5.2% for the velocities. The RMSE values are higher for the sheared cases due to the temporal variability and that the arbitrary sheared current profiles are not exactly as assumed in the theory. The results demonstrate similar performance with the focused wave interacting with a linearly sheared current and worse performance than the focused wave interacting with a uniform current. The potential reason is that uniform current profiles are better simulated than sheared current profiles. The RMSE values demonstrate good accuracy for the simulation of waves interacting with an arbitrary sheared current in both following and opposing directions.

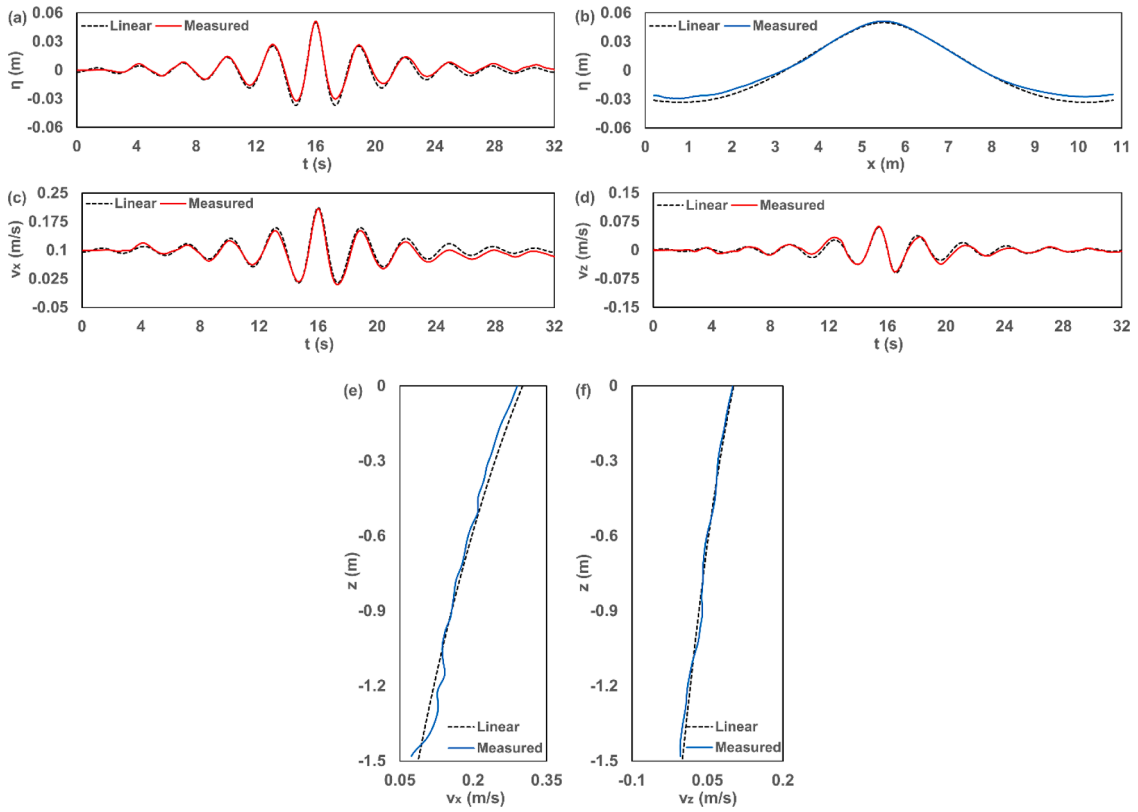

Fig. 20. Comparison between theoretical and numerical results for the focused wave interacting with the following linearly sheared current (a) surface elevation at x = 5.5 m, (b) surface elevation profile at t = 16 s, (c) horizontal velocity at x = 5.5 m, z/d = -1/3, (d) vertical velocity at x = 5.5 m, z/d = -1/3, (e) horizontal velocity profile at t = 16 s, (f) vertical velocity profile at t = 15.5 s.

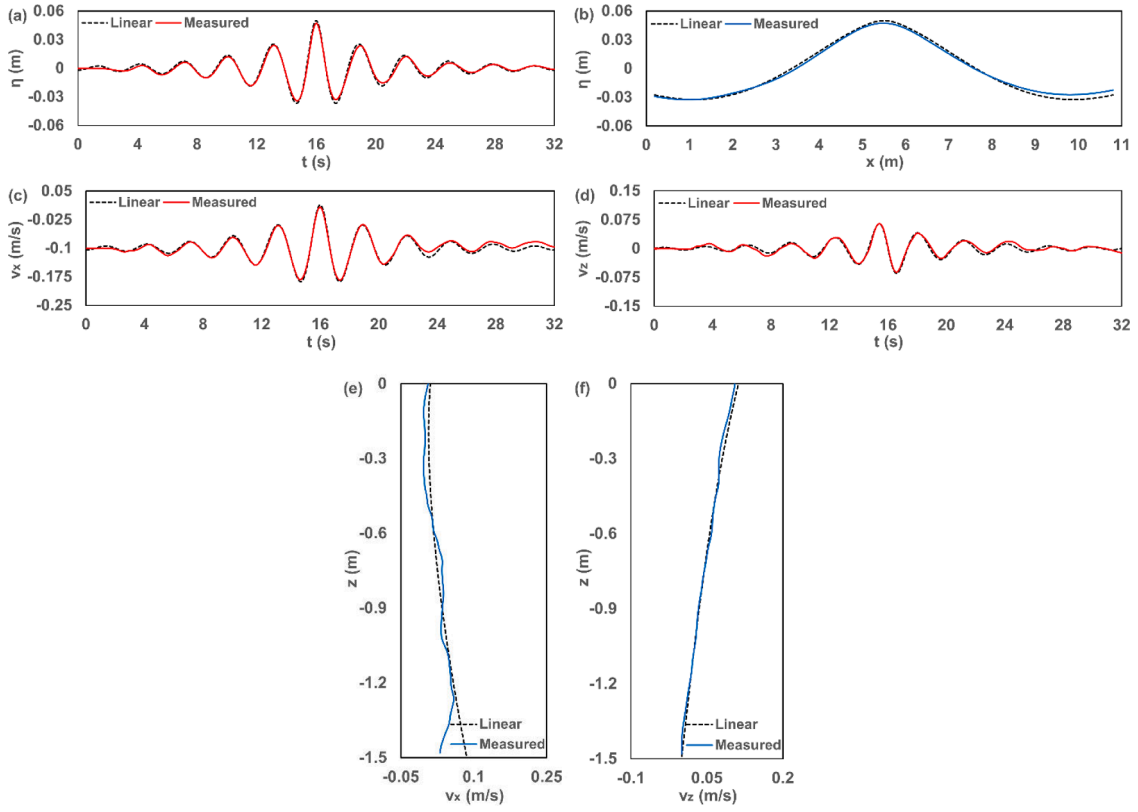

Fig. 21. Comparison between theoretical and numerical results for the focused wave interacting with the opposing linearly sheared current (a) surface elevation at x = 5.5 m, (b) surface elevation profile at t = 16 s, (c) horizontal velocity at x = 5.5 m, z/d = -1/3, (d) vertical velocity at x = 5.5 m, z/d = -1/3, (e) horizontal velocity profile at t = 16 s, (f) vertical velocity profile at t = 15.5 s.

Table 7
RMSE values of the focused wave interacting with the linearly sheared current.

	Focused wave in the following current	Focused wave in the opposing current
$RMSE(\eta(x))$	0.056	0.047
$RMSE(v_x(t))$	0.034	0.055
$RMSE(v_z(t))$	0.040	0.030

6. Discussion and conclusions

A novel numerical wave-current flume using SPH-based DualSPHysics has been introduced with open boundary conditions enabling the analytical definition of wave-current conditions. Regular, irregular and focused waves, currents and wave-current conditions are generated. For wave-current interactions, a superposition of the current profile and current altered wave velocities is imposed at the inlet and the current profile is achieved in the computational domain and the outlet simultaneously. Combined with open boundaries, a modified damping zone applied to the vertical velocity component is used for wave absorption providing access for particles to leave or enter the computational domain simultaneously when a current exists. By using this combination in the numerical wave-current flume, the required physical quantities for the generation of wave-current conditions or waves-alone and current-alone conditions are easily implemented.

Focused waves interacting with uniform current, linearly sheared current and arbitrary sheared current in both following and opposing directions were tested. The comparisons between theoretical and numerical results demonstrate good performance for all conditions. The maximum RMSE value based on the time series of surface elevation is 5.6% for the wave-current interaction tests. The maximum RMSE values based on the horizontal velocity profile and the vertical velocity profile are 5.5% and 5.2% respectively for the wave-current interaction tests. The overall RMSE values in the velocity profile are higher for focused waves interacting with sheared current cases due to the temporal variability and that the current profiles are not exactly as assumed in the theory. For the tests with focused waves, the results showed that a small domain length ($L_{domain}/L_p \approx 1.1$) is sufficient for accurate simulations.

In the present study, the accurate definition of linear boundary conditions at the inlet by using a superposition of the current profile and current altered wave velocities in this numerical wave-current flume avoids a domain for wave-current interaction to become established with associated setup time and enables effective definition of the combined wave-current field including wave amplitudes in the presence of current. With the use of a modified damping zone combined with open boundaries, only the current profile is specified at the outlet. Meanwhile, using focused waves allows for the accurate specification and generation of steep and breaking wave cases as long as the waves at the boundary are approximately linear. For wave-current interactions, the correct dispersion relations have been used to calculate the initial phases and implemented effectively in the boundary conditions as indicated by the correct focusing of wave groups at the specified point in time and space. Future work will focus on higher-order wave-current boundary conditions at the inlet for the generation of steep wave conditions.

The use of the theory of Li and Ellingsen (2019) for waves in arbitrary sheared currents allows accurate focusing and definition for complex wave-current conditions, and in combination with the open boundaries and the modified damping zone gives a powerful and flexible numerical wave-current flume. The validation in the present study enables confidence in future work aiming to assess the loading and response of offshore systems in wave-current conditions including breaking waves.

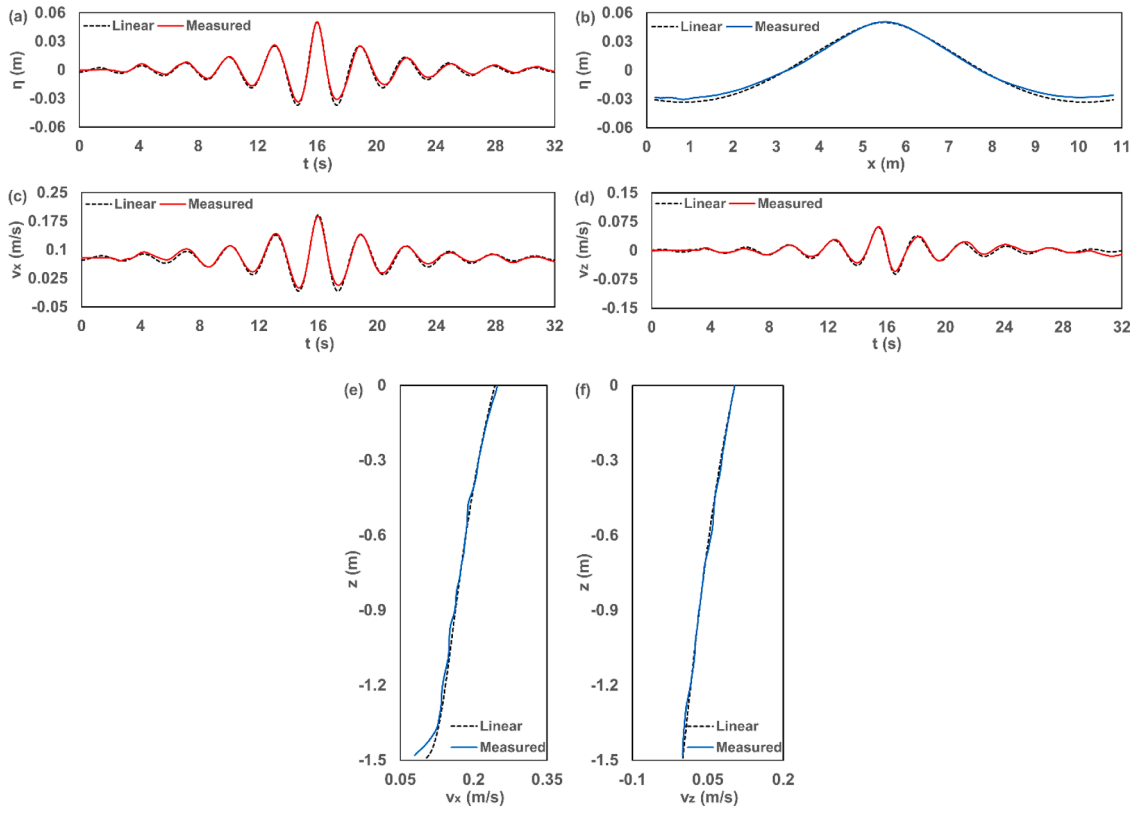

Fig. 22. Comparison between theoretical and numerical results for the focused wave interacting with the following arbitrary sheared current (a) surface elevation at $x = 5.5$ m, (b) surface elevation profile at $t = 16$ s, (c) horizontal velocity at $x = 5.5$ m, z/d = -1/3, (d) vertical velocity at $x = 5.5$ m, z/d = -1/3, (e) horizontal velocity profile at $t = 16$ s, (f) vertical velocity profile at $t = 15.5$ s.

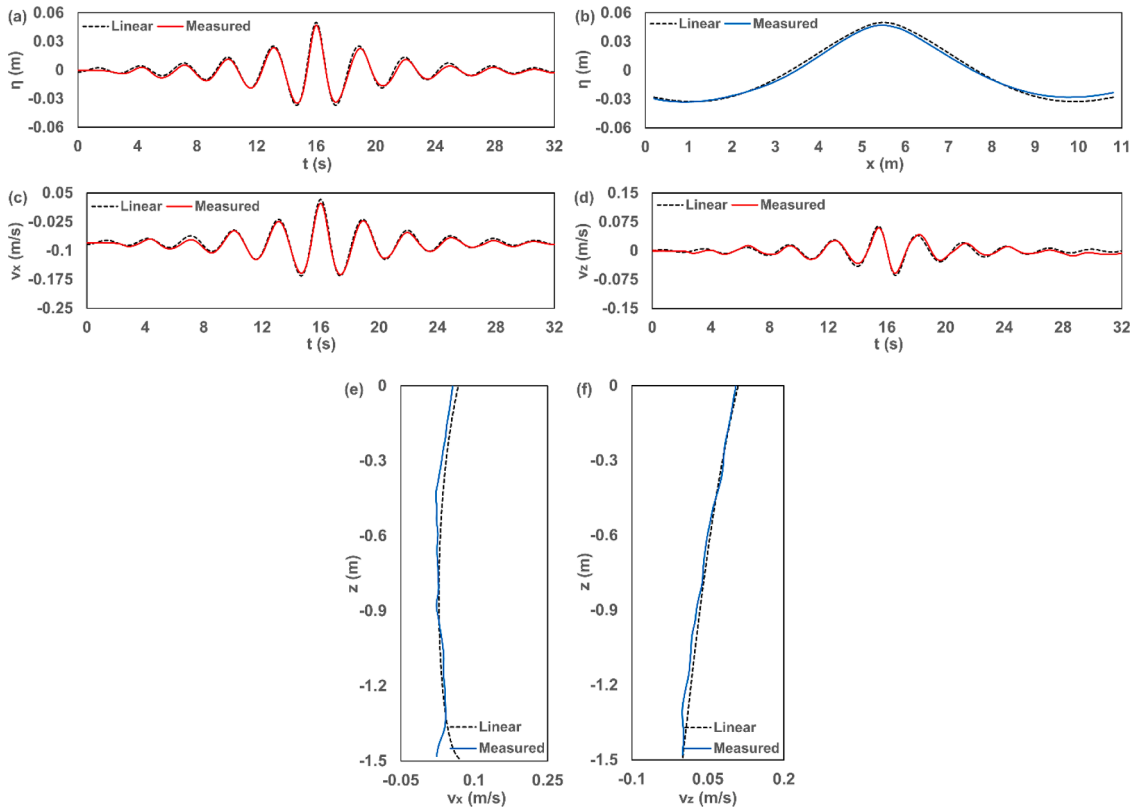

Fig. 23. Comparison between theoretical and numerical results for the focused wave interacting with the opposing arbitrary sheared current (a) surface elevation at $x = 5.5$ m, (b) surface elevation profile at $t = 16$ s, (c) horizontal velocity at $x = 5.5$ m, z/d = -1/3, (d) vertical velocity at $x = 5.5$ m, z/d = -1/3, (e) horizontal velocity profile at $t = 16$ s, (f) vertical velocity profile at $t = 15.5$ s.

Table 8
RMSE values of the focused wave interacting with the arbitrary sheared current.

	Focused wave in the following current	Focused wave in the opposing current
$RMSE(\eta(x))$	0.049	0.054
$RMSE(v_x(t))$	0.023	0.051
$RMSE(v_z(t))$	0.020	0.052

CRediT authorship contribution statement

Yong Yang: Conceptualization, Methodology, Software, Formal analysis, Validation, Investigation, Writing – original draft, Writing – review & editing. **Samuel Draycott:** Conceptualization, Methodology, Resources, Funding acquisition, Writing – review & editing, Supervision. **Peter K. Stansby:** Conceptualization, Methodology, Software, Resources, Writing – review & editing, Supervision. **Benedict D. Rogers:** Conceptualization, Methodology, Resources, Software, Writing – review & editing, Supervision.

Declaration of Competing Interest

The authors declare that they have no known competing financial interests or personal relationships that could have appeared to influence the work reported in this paper.

Data availability

Data will be made available on request.

Acknowledgments

The authors would like to acknowledge funding for this project from the Department of Mechanical, Aerospace and Civil Engineering at The University of Manchester. S. Draycott acknowledges a Dame Kathleen Ollerenshaw Fellowship. The authors would like to thank Dr Yan Li at the University of Bergen for their help in implementing the arbitrary shear boundary conditions.

Appendix A. Modelling of the focused wave with different settings

Here, the numerical results of modelling the focused wave with different settings are given which indicate the reasons for some settings used in this numerical wave-current flume in the present study.

(1) Different damping zone length (11 m and 6 m)

The measured numerical results of surface elevation at $x = 5.5$ m for the focused wave with different damping zone length are compared with the theoretical solutions in Fig. A.1. It can be found that a damping zone length longer than 6 m is required and 11m ($L_{damping}/L_p \approx 1.1$) is acceptable for this test in this numerical wave-current flume.

(2) Different equation of state (Morris and Tait)

The measured numerical results of vertical velocity at $x = 5.5$ m, z/d = -1/3 for the focused wave with different equation of state are compared with

the theoretical solutions in Fig. A.2. It can be found that Morris' equation of state Eq. (12) gives a more accurate result for the same value of the reference speed of sound $c_0 = 109.6$ m/s than Tait's equation of state Eq. (11) in this numerical wave-current flume.

The results shown in Fig. A.2 are simulated with the speed of sound at 109.6 m/s. The error is due to a spurious compressibility effect. The results show that changing the speed of sound (for example, at 175.4 m/s) can solve the issue, and it can give similar results compared with using Morris' equation of state with the speed of sound at 109.6 m/s. The measured numerical results of vertical velocity at $x = 5.5$ m, $z/d = -1/3$ for the focused wave with different equation of state using different speed of sound are compared with the theoretical solutions in Fig. A.3.

(3) Different speed of sound (109.6 m/s and 43.8 m/s)

The measured numerical results of vertical velocity at $x = 5.5$ m, $z/d = -1/3$ for the focused wave with different speed of sound are compared with the theoretical solutions in Fig. A.4. It can be found that speed of sound at 109.6 m/s gives a more stable results for this test in this numerical wave-current flume (in the present study, 109.6 m/s is used in the irregular wave test, the focused wave test and the wave-current interaction tests, 77.5 m/s is used in the regular wave test due to the smaller depth). These results indicate a sensitivity to the compressibility of the fluid.

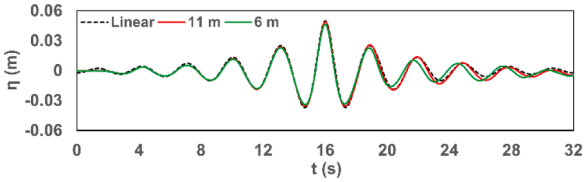

Fig. A.1. Comparison between theoretical and numerical results of surface elevation at $x = 5.5$ m for the focused wave.

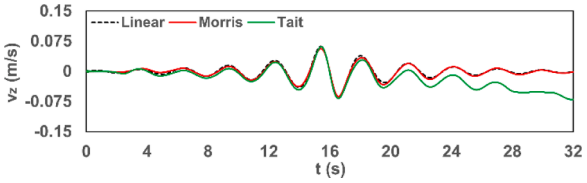

Fig. A.2. Comparison between theoretical and numerical results of vertical velocity at $x = 5.5$ m, $z/d = -1/3$ for the focused wave.

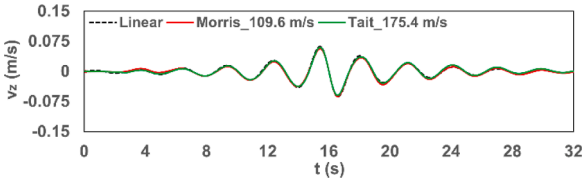

Fig. A.3. Comparison between theoretical and numerical results of vertical velocity at $x = 5.5$ m, $z/d = -1/3$ for the focused wave using different speeds of sound in different equations of state.

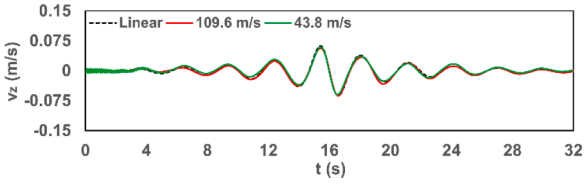

Fig. A.4. Comparison between theoretical and numerical results of vertical velocity at $x = 5.5$ m, $z/d = -1/3$ for the focused wave.

References

Altomare, C., Crespo, A.J.C., Domínguez, J.M., Gómez-Gesteira, M., Suzuki, T., Verwaest, T., 2015. Applicability of smoothed particle hydrodynamics for estimation of sea wave impact on coastal structures. Coast. Eng. 96, 1–12.

Altomare, C., Domínguez, J.M., Crespo, A.J.C., González–Cao, J., Suzuki, T., Gómez–Gesteira, M., Troch, P., 2017. Long-crested wave generation and absorption for SPH-based DualSPHysics model. Coast. Eng. 127, 37–54.

Antuono, M., Colagrossi, A., Marrone, S., Molteni, D., 2010. Free-surface flows solved by means of SPH schemes with numerical diffusive terms. Comput. Phys. Commun. 181, 532–549.

Antuono, M., Colagrossi, A., Marrone, S., 2012. Numerical diffusive terms in weakly-compressible SPH schemes. Comput. Phys. Commun. 183, 2570–2580.

Baddour, R.E., Song, S., 1990. On the interaction between waves and currents. Ocean Eng 17, 1–21.

Bruserud, K., Haver, S., Myrhaug, D., 2018. Joint description of waves and currents applied in a simplified load case. Mar. Struct. 58, 416–433.
Chen, L., Basu, B., 2019. Wave-current interaction effects on structural responses of floating offshore wind turbines. Wind Energy 22, 327–339.
Chen, H., Zou, Q., 2019. Effects of following and opposing vertical current shear on nonlinear wave interactions. Appl. Ocean Res. 89, 23–35.
Choi, W., 2009. Nonlinear surface waves interacting with a linear shear current. Math. Comput. Simul. 80, 29–36.
Crespo, A.J.C., Gómez-Gesteira, M., Dalrymple, R.A., 2007. Boundary conditions generated by dynamic particles in SPH methods. Comput. Mater. Contin. 5, 173–184.
Dalrymple, R.A., Rogers, B.D., 2006. Numerical modeling of water waves with the SPH method. Coast. Eng. 53, 141–147.
Domínguez, J.M., Fourtakas, G., Altomare, C., Canelas, R.B., Tafuni, A., García-Feal, O., Martínez-Estévez, I., Mokos, A., Vacondio, R., Crespo, A.J.C., Rogers, B.D., Stansby, P.K., Gómez-Gesteira, M., 2022. DualSPHysics: from fluid dynamics to multiphysics problems. Comput. Part. Mech. 9, 867–895.
Dong, Z., Kirby, J.T., 2012. Theoretical and numerical study of wave-current interaction in strongly-sheared flows. In: Lynett, P., Smith, J.M. (Eds.), Proceedings of 33rd Conference on Coastal Engineering. Santander, Spain.
Ellingsen, S.Å., Li, Y., 2017. Approximate dispersion relations for waves on arbitrary shear flows. J. Geophys. Res. Oceans 122, 9889–9905.
English, A., Domínguez, J.M., Vacondio, R., Crespo, A.J.C., Stansby, P.K., Lind, S.J., Chiapponi, L., Gómez-Gesteira, M., 2022. Modified dynamic boundary conditions (mDBC) for general-purpose smoothed particle hydrodynamics (SPH): application to tank sloshing, dam break and fish pass problems. Comput. Part. Mech. 9, 911–925.
Fourtakas, G., Dominguez, J.M., Vacondio, R., Rogers, B.D., 2019. Local uniform stencil (LUST) boundary condition for arbitrary 3-D boundaries in parallel smoothed particle hydrodynamics (SPH) models. Comput. Fluids 190, 346–361.
Gingold, R.A., Monaghan, J.J., 1977. Smoothed particle hydrodynamics: theory and application to non-spherical stars. Mon. Not. R. Astron. Soc. 181, 375–389.
Gómez-Gesteira, M., Rogers, B.D., Dalrymple, R.A., Crespo, A.J.C., 2010. State-of-the-art of classical SPH for free-surface flows. J. Hydraul. Res. 48, 6–27.
Gotoh, H., Khayyer, A., 2016. Current achievements and future perspectives for projection-based particle methods with applications in ocean engineering. J. Ocean Eng. Mar. Energy 2, 251–278.
Hasselmann, K., Barnett, T.P., Bouws, E., Carlson, H., Cartwright, D.E., Enke, K., Ewing, J.A., Gienapp, H., Hasselmann, D.E., Kruseman, P., Meerburg, A., Müller, P., Olbers, D.J., Richter, K., Sell, W., Walden, H., 1973. Measurements of wind-wave growth and swell decay during the joint north sea wave project (JONSWAP). Deut. Hydrogr. Z. Reihe A 8 (12).
He, M., Gao, X., Xu, W., 2018. Numerical simulation of wave-current interaction using the SPH method. J. Hydrodyn. 30, 535–538.
Jonsson, I.G., Skougaard, C., Wang, J.D., 1970. Interaction between waves and currents. Proceedings of 33rd Conference on Coastal Engineering. American Society of Civil Engineers (ASCE), Washington, D.C., pp. 489–507
Jonsson, I.G., 1990. Wave-current interactions. In: LeMehaute, B., Hanes, D.M. (Eds.), The Sea, Ocean Engineering Science. Wiley-Interscience publications, New York, pp. 65–120 vol. 9Ch. 7.
Li, Y., Ellingsen, S.Å., 2019. A framework for modeling linear surface waves on shear currents in slowly varying waters. J. Geophys. Res. Oceans 124, 2527–2545.
Lind, S.J., Xu, R., Stansby, P.K., Rogers, B.D., 2012. Incompressible smoothed particle hydrodynamics for free-surface flows: a generalised diffusion-based algorithm for stability and validations for impulsive flows and propagating waves. J. Comput. Phys. 231, 1499–1523.
Liu, M.B., Liu, G.R., 2006. Restoring particle consistency in smoothed particle hydrodynamics. Appl. Numer. Math. 56, 19–36.
Liu, X., Li, S., Ji, Z., Wu, Q., 2021. SPH simulation of hydrodynamic responses for two novel types of silt curtain under combined wave-current conditions. Appl. Ocean Res. 117, 102906.
Lucy, L.B., 1977. A numerical approach to the testing of the fission hypothesis. Astron. J. 82, 1013–1024.
Ma, Y., Ma, X., Perlin, M., Dong, G., 2013. Extreme waves generated by modulational instability on adverse currents. Phys. Fluids 25, 114109.
Markus, D., Hojjat, M., Wüchner, R., Bletzinger, K.-U., 2013. A CFD approach to modeling wave-current interaction. Int. J. Offshore Polar Eng. 23, 29–32.
Marrone, S., Antuono, M., Colagrossi, A., Colicchio, G., Le Touzé, D., Graziani, G., 2011. δ-SPH model for simulating violent impact flows. Comput. Methods Appl. Mech. Engrg. 200, 1526–1542.
Monaghan, J.J., 1992. Smoothed particle hydrodynamics. Annu. Rev. Astron. Astrophys. 30, 543–574.
Monaghan, J.J., 1994. Simulating free surface flows with SPH. J. Comput. Phys. 110, 399–406.
Monaghan, J.J., Kos, A., 1999. Solitary waves on a Cretan beach. J. Waterw. Port Coast. Ocean Eng. 125, 145–154.
Monaghan, J.J., Cas, R.A.F., Kos, A.M., Hallworth, M., 1999. Gravity currents descending a ramp in a stratified tank. J. Fluid Mech. 379, 39–69.
Ni, X., Feng, W., Huang, S., Zhang, Y., Feng, X., 2018. A SPH numerical wave flume with non-reflective open boundary conditions. Ocean Eng 163, 483–501.
Ni, X., Feng, W., Huang, S., Hu, Z., Liu, Y., 2020. An SPH wave-current flume using open boundary conditions. J. Hydrodyn. 32, 536–547.
Nwogu, O.G., 2009. Interaction of finite-amplitude waves with vertically sheared current fields. J. Fluid Mech. 627, 179–213.
Olabarrieta, M., Medina, R., Castanedo, S., 2010. Effects of wave-current interaction on the current profile. Coast. Eng. 57, 643–655.
Shadloo, M.S., Oger, G., Le Touzé, D., 2016. Smoothed particle hydrodynamics method for fluid flows, towards industrial applications: motivations, current state, and challenges. Comput. Fluids 136, 11–34.
Shi, Y., Li, S., Chen, H., He, M., Shao, S., 2018. Improved SPH simulation of spilled oil contained by flexible floating boom under wave-current coupling condition. J. Fluids Struct. 76, 272–300.
Silva, M.C., Vitola, M.A., Esperança, P.T.T., Sphaier, S.H., Levi, C.A., 2016. Numerical simulations of wave-current flow in an ocean basin. Appl. Ocean Res. 61, 32–41.
Smith, J.M., 1997. One-dimensional Wave-Current Interaction. Tech. Rep. 9. US Army Engineer Waterways Experiment Station, Coastal Engineering Research Center. Engineer Research and Development Center Vicksburg MS Coastal and Hydraulics Lab.
Steer, J.N., Borthwick, A.G.L., Stagonas, D., Buldakov, E., van den Bremer, T.S., 2020. Experimental study of dispersion and modulational instability of surface gravity waves on constant vorticity currents. J. Fluid Mech. 884, A40.
Sun, P., Ming, F., Zhang, A., 2015. Numerical simulation of interactions between free surface and rigid body using a robust SPH method. Ocean Eng. 98, 32–49.
Swan, C., Cummins, I.P., James, R.L., 2001. An experimental study of two-dimensional surface water waves propagating on depth-varying currents. Part 1. Regular waves. J. Fluid Mech. 428, 273–304.
Tafuni, A., Domínguez, J.M., Vacondio, R., Crespo, A.J.C., 2018. A versatile algorithm for the treatment of open boundary conditions in smoothed particle hydrodynamics GPU models. Comput. Methods Appl. Mech. Engrg. 342, 604–624.
Thomas, R., Kharif, C., Manna, M., 2012. A nonlinear Schrödinger equation for water waves on finite depth with constant vorticity. Phys. Fluids 24, 127102.
Toffoli, A., Waseda, T., Houtani, H., Kinoshita, T., Collins, K., Proment, D., Onorato, M., 2013. Excitation of rogue waves in a variable medium: an experimental study on the interaction of water waves and currents. Phys. Rev. E 87, 051201(R).
Verbrugghe, T., Domínguez, J.M., Altomare, C., Tafuni, A., Vacondio, R., Troch, P., Kortenhaus, A., 2019. Non-linear wave generation and absorption using open boundaries within DualSPHysics. Comput. Phys. Commun. 240, 46–59.
Violeau, D., Rogers, B.D., 2016. Smoothed particle hydrodynamics (SPH) for free-surface flows: past, present and future. J. Hydraul. Res. 54, 1–26.
Wendland, H., 1995. Piecewise polynomial, positive definite and compactly supported radial functions of minimal degree. Adv. Comput. Math. 4, 389–396.
Wolf, J., Prandle, D., 1999. Some observations of wave-current interaction. Coast. Eng. 37, 471–485.
Yao, A., Wu, C.H., 2005. Incipient breaking of unsteady waves on sheared currents. Phys. Fluids 17, 082104.
Ye, T., Pan, D., Huang, C., Liu, M., 2019. Smoothed particle hydrodynamics (SPH) for complex fluid flows: recent developments in methodology and applications. Phys. Fluids 31, 011301.
Zhang, X., 2005. Short surface waves on surface shear. J. Fluid Mech. 541, 345–370.
Zhang, J.-S., Zhang, Y., Jeng, D.-S., Liu, P.L.-F., Zhang, C., 2014. Numerical simulation of wave-current interaction using a RANS solver. Ocean Eng 75, 157–164.
Zhang, F., Crespo, A.J.C., Altomare, C., Domínguez, J.M., Marzeddu, A., Shang, S., Gómez-Gesteira, M., 2018. DualSPHysics: a numerical tool to simulate real breakwaters. J. Hydrodyn. 30, 95–105.